Copy 4
RM A58D21

NACA RM A58D21

RESEARCH MEMORANDUM

FLIGHT INVESTIGATION OF A FULL-SCALE AIRCRAFT EJECTOR WITH VARIOUS SPACING RATIOS AND CORRELATION WITH SMALL-SCALE TESTS

By C. Dewey Havill and Rodney C. Wingrove

Ames Aeronautical Laboratory
Moffett Field, Calif.

NATIONAL ADVISORY COMMITTEE
FOR AERONAUTICS

WASHINGTON

August 26, 1958

NATIONAL ADVISORY COMMITTEE FOR AERONAUTICS

RESEARCH MEMORANDUM

FLIGHT INVESTIGATION OF A FULL-SCALE AIRCRAFT EJECTOR WITH VARIOUS SPACING RATIOS AND CORRELATION WITH SMALL-SCALE TESTS*

By C. Dewey Havill and Rodney C. Wingrove

SUMMARY

A flight investigation was made to determine the thrust and pumping characteristics of a family of aircraft exhaust ejectors. Information was obtained on the variation of these characteristics with changes in engine power, flight Mach number, and ejector spacing ratio, and these results were compared to small-scale tests. The tests were conducted at a nominal pressure altitude of 25,000 feet.

Generally there was good correlation between these tests and model tests, and the cases where large differences occurred suggest the need for further research. Also, an optimum ejector length was obtained from these tests which would not have been predicted from available information, and which produced an increase in aircraft propulsive force of as much as 8-1/2 percent.

In addition to ejector characteristics, results were obtained showing how a swinging survey probe can be used as a device for calibrating a tail-pipe pressure probe for the measurement of thrust and air flow.

INTRODUCTION

When an aircraft engine is equipped with an afterburner using a two-position exhaust nozzle, and has an exhaust ejector to pump tail-pipe cooling air, then both diameter and spacing ratios differ for the two nozzle positions. As shown by the data of reference 1 and similar investigations, different diameter and spacing ratios can result in widely different thrust and pumping characteristics. Therefore, an

*Title, Unclassified.

ejector designed to provide adequate tail-pipe cooling and thrust characteristics during the critical afterburning condition may have severe performance losses in the cruise condition with the afterburner not operating. Such a situation is illustrated by the data of reference 2.

An ideal ejector design should provide the proper amount of tail-pipe cooling air for the afterburner-on condition, while retaining the maximum possible net thrust for both afterburner-on and afterburner-off operation. Investigations such as that reported in reference 1 were made in order to provide the information necessary to design an ejector in accordance with these requirements. However, the differences in scale, jet temperature, jet rotation, and jet velocity profiles might cause the results of the reference 1 model tests to differ from those of full-scale aircraft ejectors. In order to evaluate the magnitude of these differences the investigation reported in reference 2 was undertaken. In the present investigation, a wider range of ejector geometry was covered and a more refined temperature probe (discussed in ref. 3) which provided more reliable temperature and weight flow profiles was used. A method is described whereby this probe may be used to calibrate a fixed single point probe for obtaining net-thrust measurements.

NOTATION

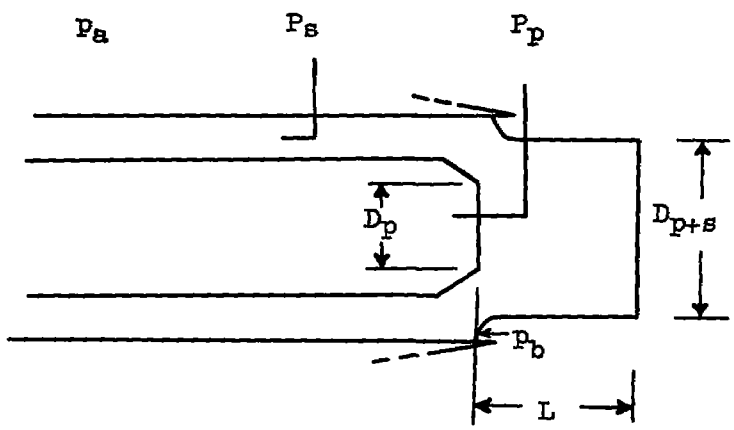

A	area, sq ft
C_F	thrust coefficient
C_W	air-flow coefficient
D	diameter, ft

$\frac{D_{p+s}}{D_p}$	diameter ratio
F_g	gross thrust, lb
$\frac{F_{g_{p+s}}}{F_{g_p}}$	gross-thrust ratio
F_n	net thrust (F_g-WV), lb
L	length from tail-pipe exit to shroud exit, ft
$\frac{L}{D_p}$	spacing ratio
M	flight Mach number
P	local total pressure, lb/ft^2
p	local static pressure, lb/ft^2
p_a	atmospheric pressure, lb/ft^2
p_b	annular base pressure, lb/ft^2
$\frac{P_p}{p_a}$	primary pressure ratio
$\frac{P_s}{p_b}$	secondary pressure ratio
R	gas constant, 1715 $ft^2/sec^2\ {}^oR$
r	distance from jet center line, ft
T	local total temperature, ^oR
V	flight velocity, ft/sec
V_j	jet velocity, ft/sec
W	air-flow rate, slugs/sec

$\frac{W_s}{W_p}\sqrt{\frac{T_s}{T_p}}$ corrected air-flow ratio

ρ_j jet density, slugs/ft^3

Subscripts

p primary system

p+s primary and secondary system combined

s secondary system

i value computed from one-dimensional flow equations

DESCRIPTION OF TEST AIRPLANE

A Lockheed F-94C airplane equipped with a J48-P8 engine with afterburner was used for this investigation. A photograph of the test airplane is shown in figure 1, a two-view drawing in figure 2, and a list of dimensions in table I. A schematic cross-sectional drawing of the ejectors is shown in figure 3. The ejector spacing ratio was changed during the investigation by the addition of cylindrical extensions of various lengths to the shroud. These changes produced the spacing ratios listed in the following table:

Engine condition	Diameter ratio	Spacing ratio				
		Basic	Modified			
Afterburner off	1.32	0.27	0.38	0.43	0.50	0.65
Afterburner on	1.12	.40	.49	.54	.60	.72

Secondary air flow was supplied through 12 submerged inlets mounted around the fuselage at 2 longitudinal locations as shown in figure 4. Each forward inlet had an inlet area of 0.045 square foot, and each rear inlet 0.026 square foot. Also shown in figure 4 is a 1/8-inch gap between the fuselage and the tail cone.

INSTRUMENTATION AND TESTS

During this investigation the following quantities were obtained: airspeed and altitude; tail-pipe (primary) pressure, thrust, and air flow; ejector pressure, thrust, and air flow; and annular base pressure. The data were recorded on standard NACA instruments supplemented by a recording oscillograph.

Airspeed and altitude were obtained from a pitot-static probe mounted on a 12-1/2-foot nose boom. This installation was calibrated against a pacer airplane. Tail-pipe pressure, used to determine thrust and air flow, was obtained from an air-cooled total pressure probe mounted at the tail-pipe exit as shown in figure 5. Standard nozzle equations given in the appendix were used to compute thrust and air flow from tail-pipe pressure and temperature. Nozzle thrust coefficient (fig. 6) was obtained from calibrations of the system, with the ejector removed, on a thrust stand. The tail-pipe temperature was assumed equal to the average temperature in the jet core region of the ejector temperature profiles (i.e., the average temperature for $r < 0.8$ foot in fig. 7). Application of equations presented in the appendix to ground calibration data and use of engine manufacturer's data for similar operating conditions indicated that nozzle air-flow coefficient could be assumed equal to nozzle thrust coefficient.

Ejector thrust and air flow were obtained by the method discussed in reference 4 using the swinging sonic-flow orifice survey probe discussed in reference 3. Operational jet pressures during this investigation were of a magnitude which permitted neglecting the static-pressure error presented in reference 4 with negligible inaccuracy in the results. A photograph of the probe mounted on the aircraft is shown in figure 5. Typical pressure and temperature profiles obtained during an ejector exit survey are presented in figure 7. Figure 8 presents thrust and air-flow profiles computed from the data shown in figure 7. Integration of the profiles in figure 8 over the ejector area yields ejector gross thrust and air flow. Ejector area measured with the engine shut down was used for the integration limit. Since the swinging survey probe covers only one cross section of a jet, there exists some doubt as to whether this cross section is representative of the entire jet. Calibrations were made on a thrust stand to check the validity of the present swinging probe installation as a thrust measuring device, and a nozzle thrust coefficient was computed. This coefficient is presented in figure 6 and indicates that a 2-percent correction must be applied to the thrust measurement. The data contained herein have had this correction applied to all thrust and air-flow data.

It is difficult to determine the error inherent in these data with any great degree of confidence, since the assumed extensions of ground calibrations to flight conditions might possibly lead to a greater

magnitude of error than all other sources of error combined. However, if the effect of temperature error is neglected, and the extrapolation of ground calibrations to flight conditions is assumed valid, the error in primary and ejector thrust and air flow would be estimated at 1 to 2 percent. The effect of error in temperature measurement would be to increase the error in air flows. However, since the jet temperature measured by the swinging probe is used to compute both primary and ejector air flows, the effect of an error in temperature on the ratio (W_{p+s}/W_p) should be negligible. The secondary air-flow ratio is obtained from the following equation:

$$\frac{W_s}{W_p}\sqrt{\frac{T_s}{T_p}} = \left(\frac{W_{p+s}}{W_p} - 1\right)\sqrt{\frac{T_s}{T_p}}$$

For the present data, an error of 1 percent in (W_{p+s}/W_p) would produce an error of about 0.01 in (W_s/W_p) in addition to the effect of errors in $\sqrt{T_s/T_p}$. The value of T_s was determined by inspection of the ejector temperature profiles, and was taken as the temperature immediately inside the ejector shroud. An error of 10° F in T_s or an error of 30° F in T_p would result in an error of less than 1 percent in the value of $(W_s/W_p)\sqrt{T_s/T_p}$. Since T_s and T_p are measured with the same device, and since the measuring error is thought to be less than the above values, the error in $(W_s/W_p)\sqrt{T_s/T_p}$, due to temperature error, is thought to be negligible.

For some regions in figure 7, static pressure is greater than total pressure, which implies flow into the ejector. However, ground tests and visual inspection of the ejector indicated that such reverse flow did not occur. Therefore the static-pressure measurement was assumed to be in error because of the effects of jet and airplane pressure fields, and the fact that the static-pressure measurement was not made in the plane of the ejector exit. Where this condition occurred, the true static pressure was chosen equal to the measured total pressure. Since positive values of $(p_{p+s}-P_{p+s})$ were generally small, the error due to this choice should not be large.

The secondary pressure was obtained with three total pressure probes mounted 120° apart, an inch from the shroud wall near the plane of the tail-pipe nozzle. The probes were manifolded and the pressure measured with a 0 to 1 pound per square inch differential pressure cell referred to the nose-boom static-pressure system. Annular base pressure was obtained in the same manner.

Tests were made at an altitude of 25,000 feet over a Mach number range from 0.50 to 0.92. The airplane was operated over the Mach number range, first with just sufficient power for level flight, then with maximum nonafterburning power, and finally with the afterburner on; thus

three variations of primary flow conditions with Mach number were obtained. Primary temperatures for the three variations were 1550° R to 1800° R, 1800° R, and 3000° R, respectively. Primary total pressure ratio is plotted against Mach number for the three operating conditions in figure 9.

RESULTS AND DISCUSSION

Test Results

Ejector thrust ratios, corrected air-flow ratios, and the ratio of secondary total pressure to base pressure are presented in figures 10, 11, and 12 for all of the ejector configurations tested. Gross-thrust ratio, air-flow ratio, and net-thrust ratio are cross-plotted against spacing ratio in figures 13, 14, and 15. In the computation of ejector net thrust, the ejector was charged with the total loss in secondary air-flow pressure from free-stream conditions to ejector exit. Figure 15 shows that an appreciable performance gain can be realized by optimization of the ejector. For example, sealing the fuselage gap and increasing the ejector shroud length 2.4 inches (L/D_p = 0.27 to L/D_p = 0.38, afterburner off) increased the aircraft net thrust as much as 8-1/2 percent with the afterburner off and 6 percent with the afterburner on, while more than the original quantity of secondary air flow for tail-pipe cooling was maintained. The following example indicates the importance of this improvement on aircraft fuel economy. During all flights reported herein, a measurement was obtained of the fuel used to take off, climb, and accelerate to the test altitutde and speed. An attempt was made to follow the same flight procedure in all cases, but minor variations in technique and atmospheric conditions caused the results of these measurements to be only qualitative. The information so obtained indicated that optimizing the ejector caused a reduction in fuel consumption of the order of 25 to 30 percent for these maneuvers.

Comparison With Model Tests

Model data from reference 1 are presented in figures 10, 11, and 12. Thrust ratios were determined in the manner indicated by an errata on reference 1. In order to obtain data at a diameter ratio of 1.32 from reference 1, a linear interpolation was made between the diameter ratios 1.21 and 1.40.

Thrust and air-flow ratios for ejectors are dependent on the pressure into which the ejector exhausts, with this quantity forming the denominator of secondary pressure ratio. Since fuselage shape, Mach number, and the jet all affect the pressure into which the ejector exhausts, it is

difficult to determine where to measure that pressure in a flight investigation. For the present investigation, that pressure was measured in the annular base region so that it would be unaffected by the jet for all but the shortest spacing ratio configuration.

For each configuration shown in figures 10, 11, and 12, the average difference between flight and model data is plotted in figure 16. For the afterburner off (figs. 16(a) and 16(b)), good correlation was obtained between the model data and flight tests for spacing ratios of 0.38, 0.43, 0.50, and 0.65, the over-all average difference being less than 1-1/2 percent. For the shortest spacing ratio, model data indicate 4 to 5 percent higher thrust and air-flow ratios. For this spacing ratio the measured base pressure was 2 percent less than for the longer spacing ratios, and the decrease is believed to be due to jet effect. If base pressure were adjusted to conform with that measured at the longer spacing ratios, then a 5-percent change in the thrust and air-flow ratios predicted from model data would result, and good correlation would be obtained for the shortest spacing ratio also.

For the afterburner-on data (fig. 16(c)) there appear to be more serious discrepancies between model and flight results. At the longest spacing ratio, model-thrust ratio is 6 percent higher than flight-thrust ratio, while model air-flow ratio is 5 percent lower than flight air-flow ratio. The nature of these differences (opposite in sign) indicates the possibility of premature choking in the flight ejector, due possibly to jet rotation which is not present in model tests. For any ejector configuration, there is a critical primary pressure at which the jet expands to just fill the ejector exit. When this occurs, a large drop in ejector thrust results accompanied by a large increase in ejector air flow. With an appreciable amount of jet rotation, there might be a tendency for this condition to occur at a slightly lower primary pressure ratio and to produce a larger decrease in thrust and increase in air flow. For the lowest afterburner-on spacing ratio, model tests predict an ejector thrust ratio 7-1/2 percent higher than was obtained. For a spacing ratio this short, it is possible that primary nozzle geometry and boundary layer become important. In the flight installation there was no restriction at the primary nozzle exit, which was not the case in model tests. This difference might have resulted in relatively larger primary jet boundary layers for the full-scale ejector.

The foregoing differences between flight and wind-tunnel data for the afterburner-on configurations indicate the desirability of a systematic evaluation of the effects of primary jet rotation, primary nozzle geometry, and primary jet boundary layer on ejector characteristics.

The optimization of spacing ratio for peak net thrust, as discussed previously and shown in figure 15, can produce an appreciable increase in performance. For design purposes, however, an optimum spacing ratio cannot be determined unless an accurate estimation of secondary pressure

ratio is obtained. For example, if a constant secondary pressure ratio were assumed for the configurations reported here, no optimum spacing ratio would be predicted from the model data. Furthermore, in order to estimate secondary pressure ratio, both secondary flow losses and the no jet flow value of base pressure must be determined. For these reasons it appears that model data may be used to establish a preliminary ejector design, but the final design should be determined by flight tests.

Primary Probe Calibration

For many aircraft performance tests, the test program is so extensive that maintenance of a swinging probe, and the reduction of data from it, becomes impractical. Also, since several seconds are required for swinging a probe, performance measurements cannot be made during rapid changes of engine operating conditions. One solution to these problems is to use a swinging survey probe under flight conditions, in a manner comparable to the use of a thrust stand on the ground, that is, for calibrating a fixed tail-pipe probe.

The results of the fixed tail-pipe probe calibrations, for the ejectors reported herein, are shown in figure 17. Figure 17(a) presents true aircraft gross thrust divided by isentropic thrust computed from pressure measured by the fixed tail-pipe probe. Therefore, for any condition in which true thrust is desired, thrust computed from tail-pipe exit pressure is multiplied by the appropriate value of thrust coefficient taken from figure 17(a). Also plotted in figure 17(a) are the values of thrust coefficient obtained on the ground using a thrust stand. These values are the same as those shown in figure 6. In addition to extending the thrust-stand data to flight values of primary pressure ratio, and thus avoiding the necessity of extrapolating ground data, the flight data of figure 17(a) also include ejector thrust losses which could not be obtained from a ground thrust-stand calibration. If only a thrust-stand calibration were used, a curve similar to that shown in figure 17(a) would be used to compute aircraft thrust and, as can be seen from this figure, the value of thrust so computed could be in error by almost 10 percent. Figure 17(b) presents similar data for air-flow coefficient, with secondary to primary temperature ratio included. Therefore, in order to obtain the true air flow through both engine and ejector, primary and secondary temperature must be measured in addition to primary pressure. Use of the curves in figure 17 provides no information concerning the true value of engine gross thrust, net thrust, or air flow, since these curves include ejector losses and ejector air flow. However, when the computation of aircraft performance parameters, such as drag coefficient, requires a knowledge of propulsive force, then the curves of figure 17 are applicable, since the computation of thrust and air flow by means of these curves leads to the true net propulsive force on the airframe.

The only indication of the accuracy of the swinging survey probe as a thrust measuring device is the data shown in figure 6. Because the correction value shown here is small, and because it is constant over the pressure range covered, it seems logical to extend this value to flight operating conditions and, in the absence of better information, the swinging probe accuracy in determining gross thrust with the correction value of figure 6 is assumed to be 1 to 2 percent. Also, there is no reason why similar accuracies should not be obtained on other installations. If a swinging probe were used to obtain calibration curves such as those of figure 17, then on the basis of present experience the inaccuracy in obtaining net aircraft propulsive force by means of these curves would be about 4 to 5 percent. This accuracy could be expected over most ranges of flight conditions, but further difficulties would be expected with continuously varying ejector configurations, where the curves of figure 17 would be more difficult to obtain, and where inaccuracies in the measurement of ejector and primary nozzle positions would result in greater inaccuracy of thrust measurements.

CONCLUDING REMARKS

The results of this investigation indicate that there is generally good agreement between flight and model tests. For those configurations where there is more than 3-percent difference between flight and model tests, hypotheses have been advanced to explain the differences. In order to check the validity of these hypotheses, systematic studies of the effects of jet rotation, primary jet boundary layer, and primary nozzle geometry on ejector characteristics are needed.

Although flight and model tests compare favorably, the sensitivity of ejector performance to secondary pressure ratio requires an accurate knowledge of the latter quantity for prediction of the former. Therefore, unless secondary pressure and base pressure can be accurately estimated, final design of aircraft ejectors should be determined from flight tests.

Ames Aeronautical Laboratory
National Advisory Committee for Aeronautics
Moffett Field, Calif., Apr. 21, 1958

APPENDIX

THRUST AND AIR-FLOW EQUATIONS

The gross thrust over a differential element of area dA of the tail-pipe or ejector exit is given by the equation

$$dF_g = (\rho_j V_j^2 + p - p_a)dA \tag{1}$$

The corresponding equation for air-flow rate is

$$dW = \rho_j V_j dA \tag{2}$$

In order to determine total gross thrust or air-flow rate, equation (1) or (2) is integrated over the desired area. For the tail-pipe exit, any variation in ρ_j, V_j, p, or p_a over the tail-pipe exit area A_p is absorbed in an experimentally determined nozzle coefficient C_{F_p} or C_{W_p} giving the following equations:

$$F_{g_p} = C_{F_p}(\rho_p V_p^2 + p - p_a)A_p \tag{3}$$

$$W_p = C_{W_p}\rho_p V_p A_p \tag{4}$$

If it is assumed that $p = p_a$ when the nozzle is unchoked, and

$$p = P\left(\frac{2}{\gamma+1}\right)^{\frac{\gamma}{\gamma-1}}$$

when the nozzle is choked, then the following equations can be obtained from equations (3) and (4):

$$\left.\begin{aligned} F_{g_p} &= C_{F_p} \frac{2\gamma}{\gamma-1} A_p p_a \left[\left(\frac{P_p}{p_a} \right)^{\frac{\gamma-1}{\gamma}} - 1 \right] \qquad (5) \\ W_p &= C_{W_p} \frac{A_p P_p}{\sqrt{T_p}} \sqrt{\frac{2\gamma}{\gamma-1} \frac{1}{R} \left(\frac{p_a}{P_p} \right)^{\frac{\gamma+1}{\gamma}} \left[\left(\frac{P_p}{p_a} \right)^{\frac{\gamma-1}{\gamma}} - 1 \right]} \qquad (6) \end{aligned}\right\} \text{for } \left(\frac{P_p}{p_a} \right) < \left(\frac{\gamma+1}{2} \right)^{\frac{\gamma}{\gamma-1}}$$

and

$$\left.\begin{aligned} F_{g_p} &= C_{F_p} A_p P_p \left[2 \left(\frac{2}{\gamma+1} \right)^{\frac{1}{\gamma-1}} - \frac{p_a}{P_p} \right] \qquad (7) \\ W_p &= C_{W_p} \frac{A_p P_p}{\sqrt{T_p}} \sqrt{\frac{\gamma}{R} \left(\frac{2}{\gamma+1} \right)^{\frac{\gamma+1}{\gamma-1}}} \qquad (8) \end{aligned}\right\} \text{for } \left(\frac{P_p}{p_a} \right) \geq \left(\frac{\gamma+1}{2} \right)^{\frac{\gamma}{\gamma-1}}$$

To obtain ejector thrust and air flow, equations (1) and (2) are integrated over the ejector exit, so nozzle coefficients such as those used for the tail-pipe exit are not required. However, if only one cross section of the ejector exit is surveyed, then a thrust coefficient should be included to adjust for variations between this cross section and other cross sections. Then the equations for ejector gross thrust and air flow resulting from equations (1) and (2) are as follows:

$$F_{g_{p+s}} = C_{F_{p+s}} \int_0^{A_{p+s}} \left\{ \frac{2\gamma}{\gamma-1} p_{p+s} \left[\left(\frac{P_{p+s}}{p_{p+s}} \right)^{\frac{\gamma-1}{\gamma}} - 1 \right] + (p_{p+s} - p_a) \right\} dA \qquad (9)$$

$$W_{p+s} = C_{W_{p+s}} \int_0^{A_{p+s}} \left\{ \sqrt{\frac{2\gamma}{\gamma-1} \frac{P_{p+s}^2}{RT_{p+s}} \left(\frac{p_{p+s}}{P_{p+s}}\right)^{\frac{\gamma+1}{\gamma}} \left[\left(\frac{P_{p+s}}{p_{p+s}}\right)^{\frac{\gamma-1}{\gamma}} - 1 \right]} \right\} dA \quad (10)$$

where dA is the area of a circular ring of thickness dr and radius r from the jet center line.

For the present investigation, values of γ were assumed as follows:

Afterburner off	$\gamma = 1.35$
Afterburner on	$\gamma = 1.30$

REFERENCES

1. Greathouse, W. K., and Hollister, D. P.: Air-Flow and Thrust Characteristics of Several Cylindrical Cooling-Air Ejectors With a Primary to Secondary Temperature Ratio of 1.0. NACA RM E52L24, 1953. (Errata No. 1, 1957)

2. Rolls, L. Stewart, and Havill, C. Dewey: An Evaluation of Two Cooling-Air Ejectors in Flight at Transonic Speeds. NACA RM A54A05, 1954.

3. Havill, C. Dewey, and Rolls, L. Stewart: A Sonic-Flow Orifice Probe for the In-Flight Measurement of Temperature Profiles of a Jet Engine Exhaust With Afterburning. NACA TN 3714, 1956.

4. Rolls, L. Stewart, Havill, C. Dewey, and Holden, George R.: Techniques for Determining Thrust in Flight for Airplanes Equipped With Afterburners. NACA RM A52K12, 1953.

TABLE I.- DIMENSIONS OF THE TEST AIRPLANE

Wing	
Total wing area (including projected fuselage area), sq ft	232.8
Span, ft	32.6
Aspect ratio	6.1
Mean aerodynamic chord, in.	80.6
Leading-edge sweepback	$9^{\circ}18'$
Fuselage	
Length, ft	44.72
Depth (maximum), in.	56
Width (maximum), in.	56
Tail-pipe exit area	
Afterburner off, sq ft	2.73
Afterburner on, sq ft	3.81
Ejector area, sq ft	4.77

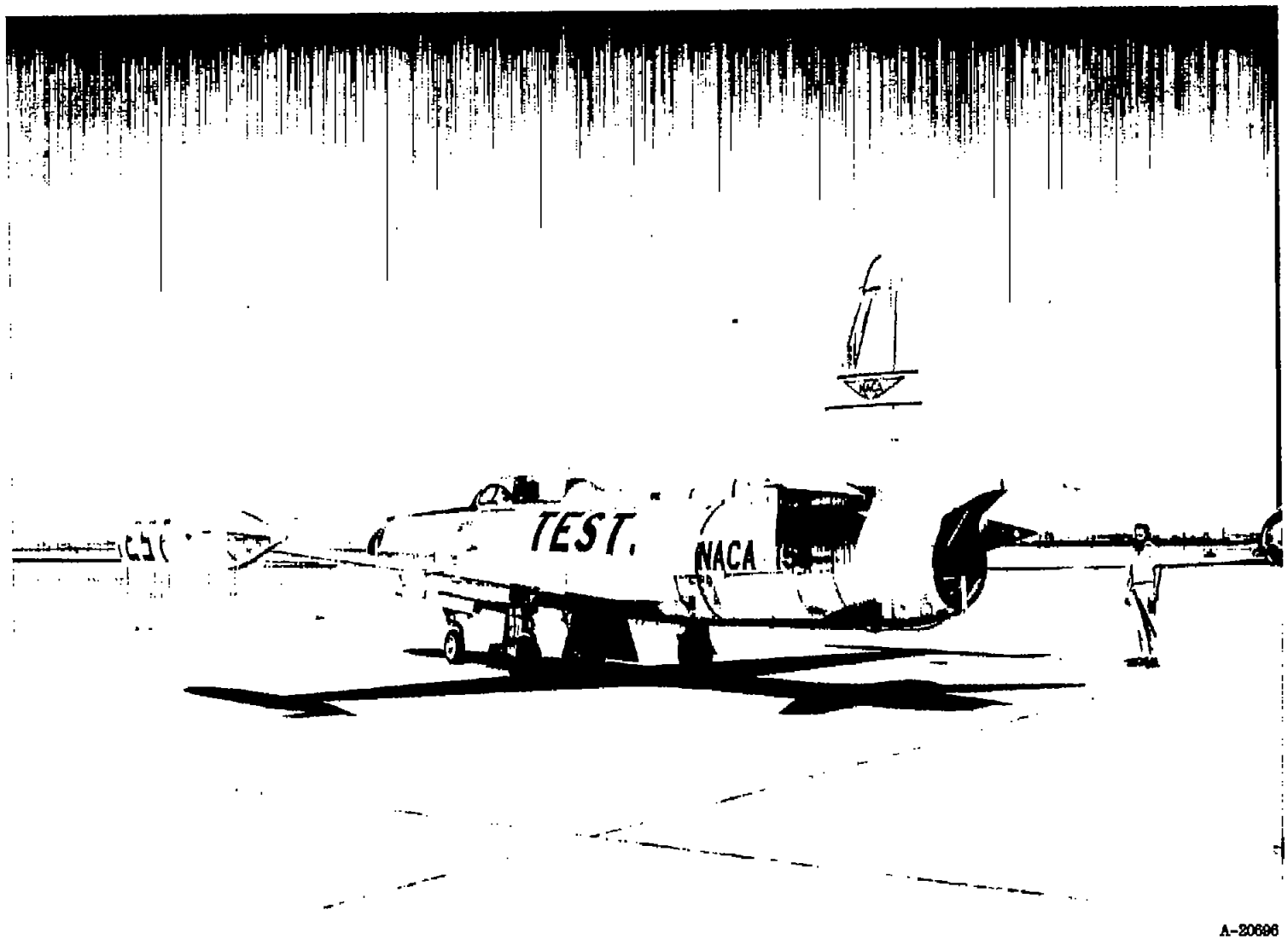

A-20696

Figure 1.- Test airplane.

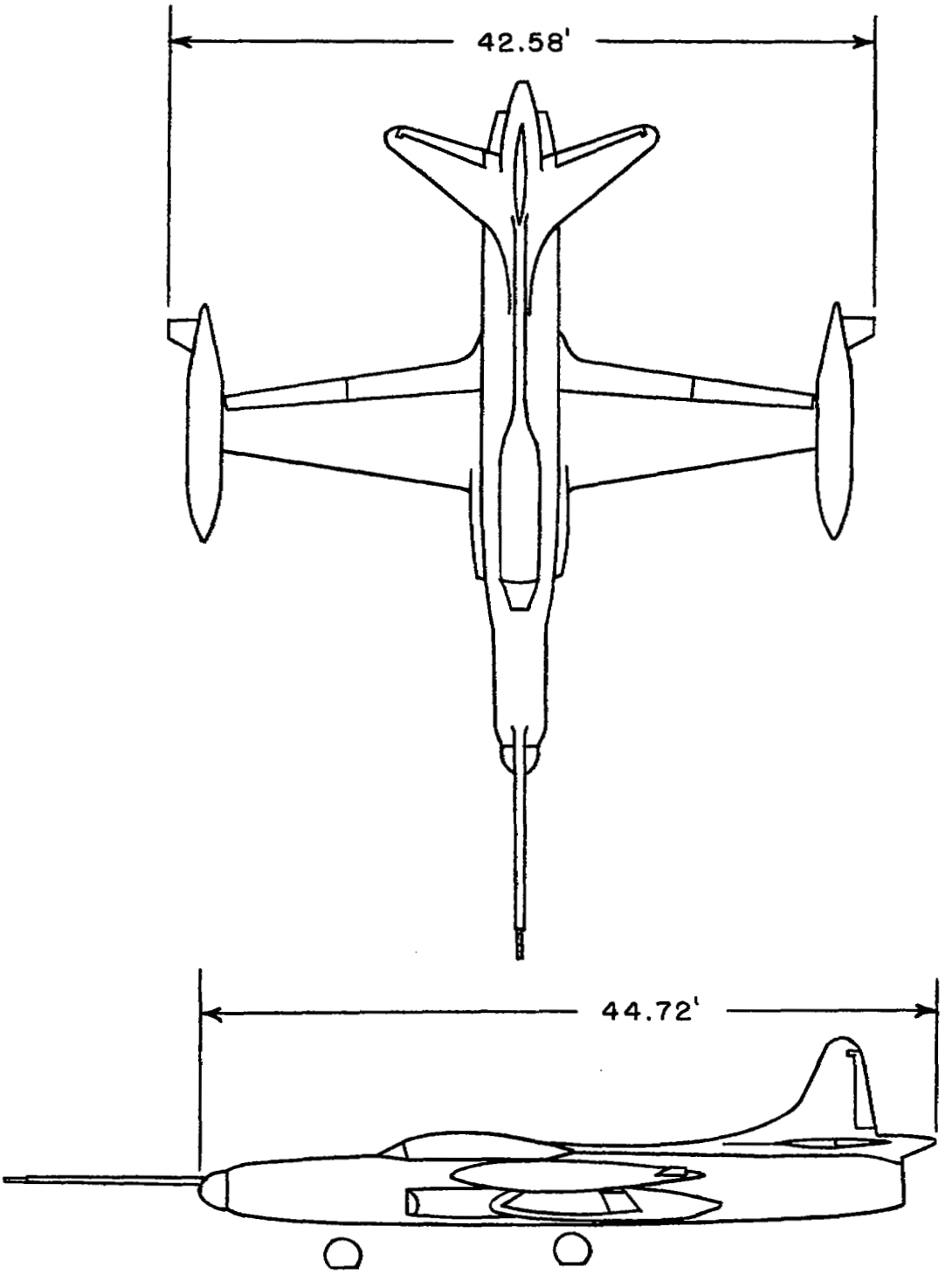

Figure 2.- Two-view drawing of test airplane.

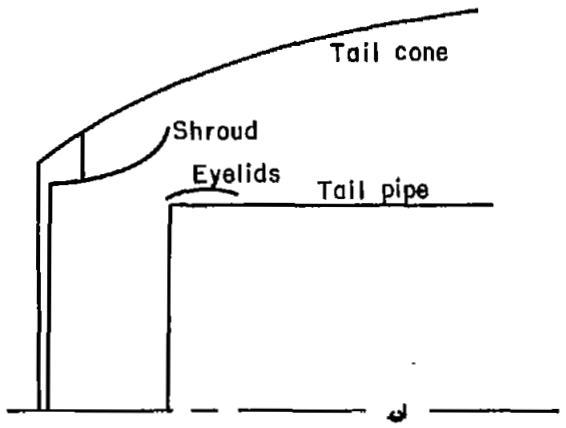

(a) Basic shroud; afterburner on.

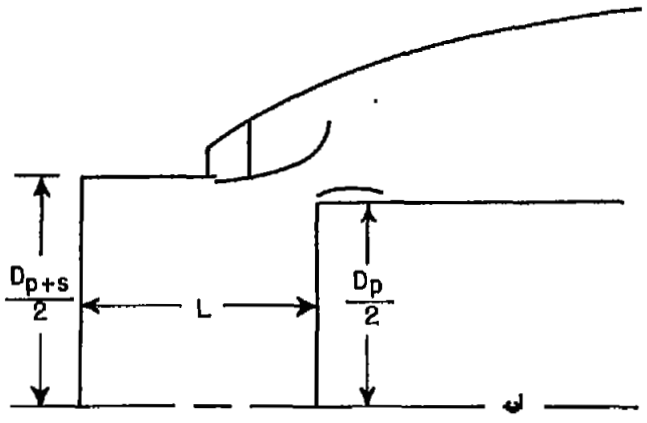

(c) Modified shroud; afterburner on.

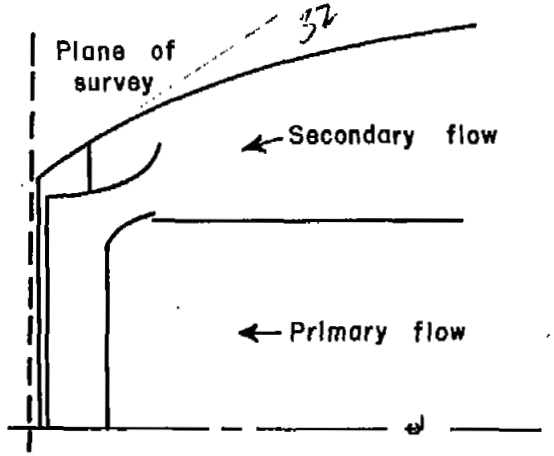

(b) Basic shroud; afterburner off.

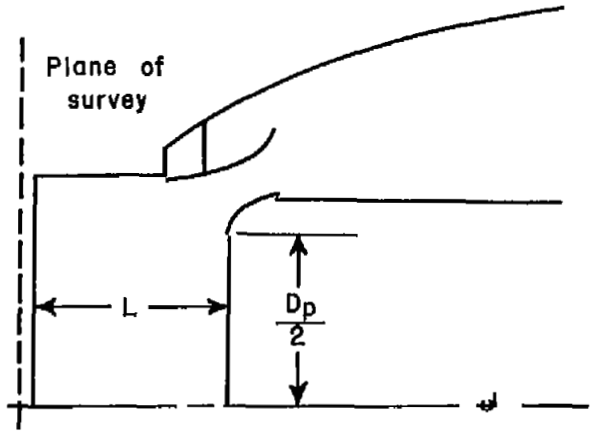

(d) Modified shroud; afterburner off.

Figure 3.- Cross-sectional drawing of the cooling air ejectors.

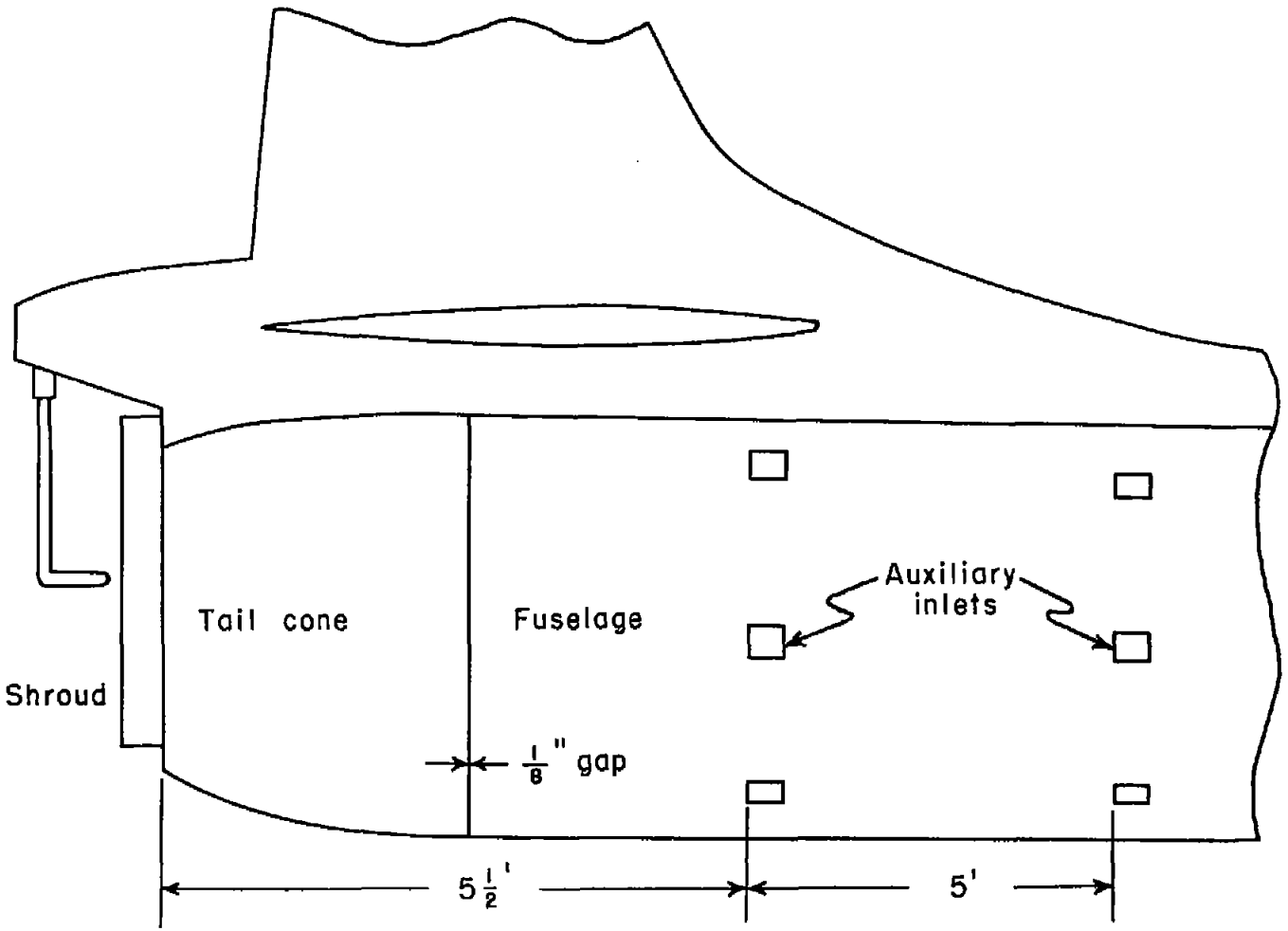

Figure 4.- Aftersection of the test airplane.

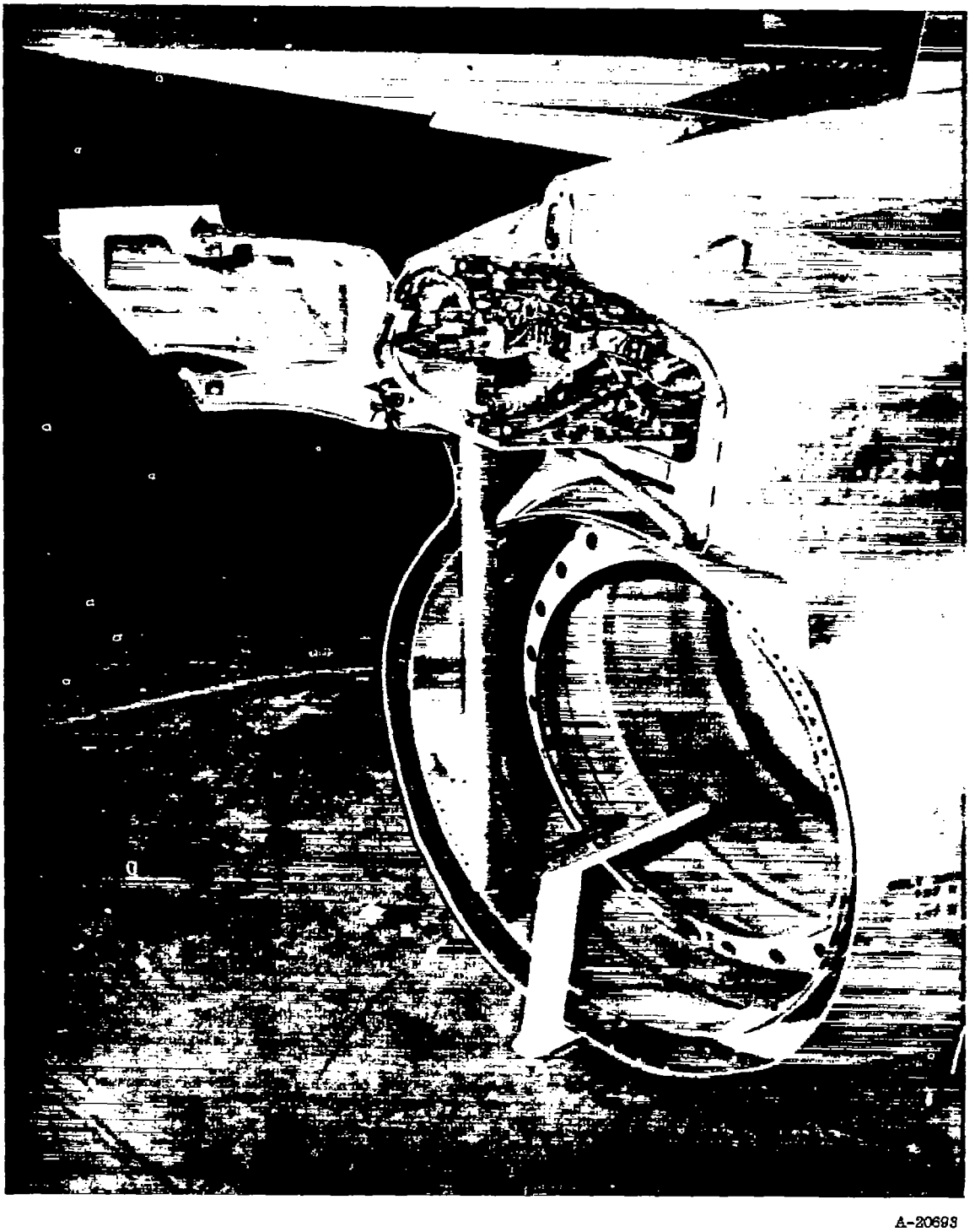

A-20693

Figure 5.- Tail-pipe exit and test instrumentation.

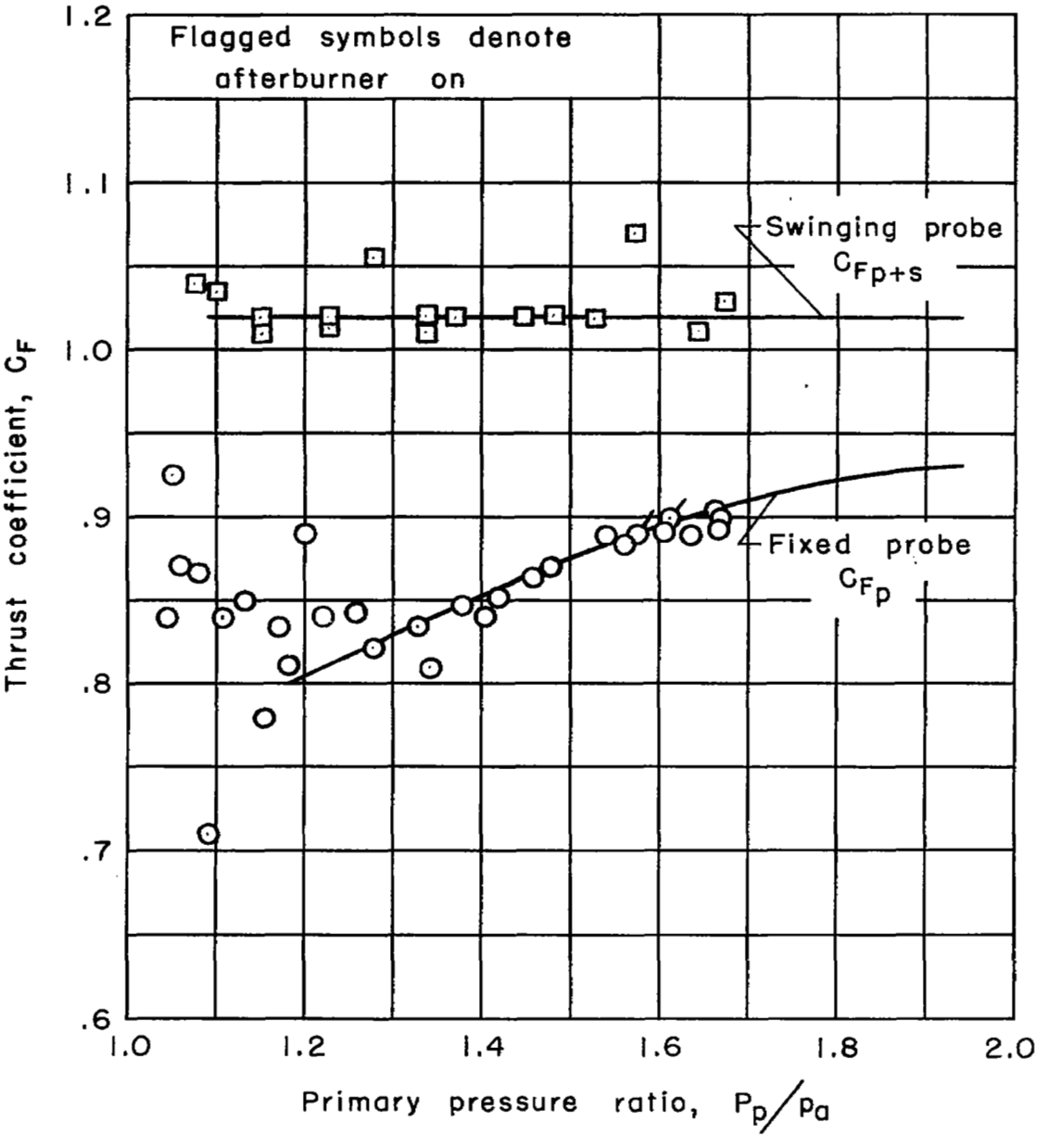

Figure 6.- Variation of the thrust coefficients with primary pressure ratio.

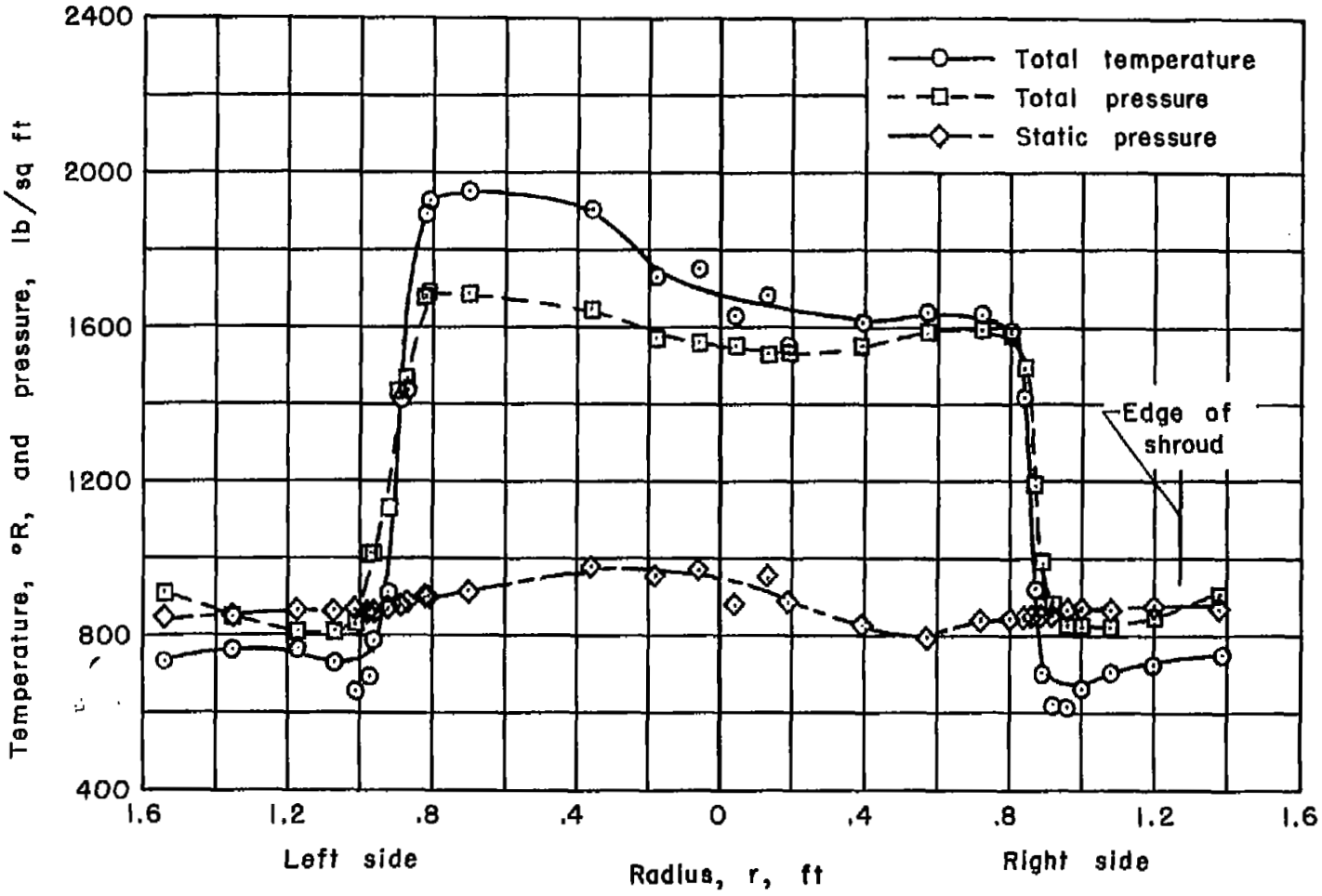

(a) Afterburner off; diameter ratio = 1.32; spacing ratio = 0.43.

Figure 7.- Typical pressure and temperature surveys at the ejector exit; M = 0.75.

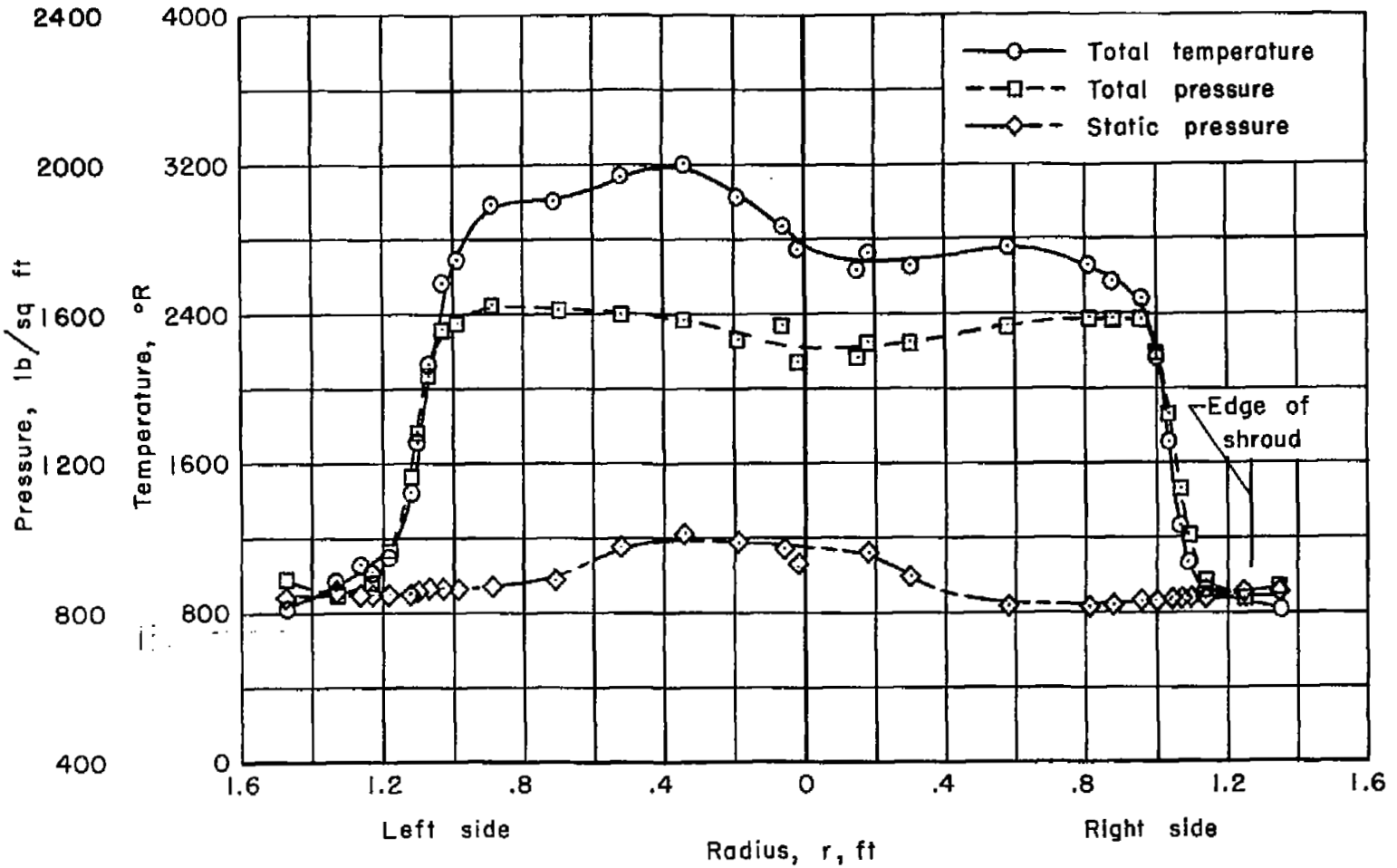

(b) Afterburner on; diameter ratio = 1.12; spacing ratio = 0.54.

Figure 7.- Concluded.

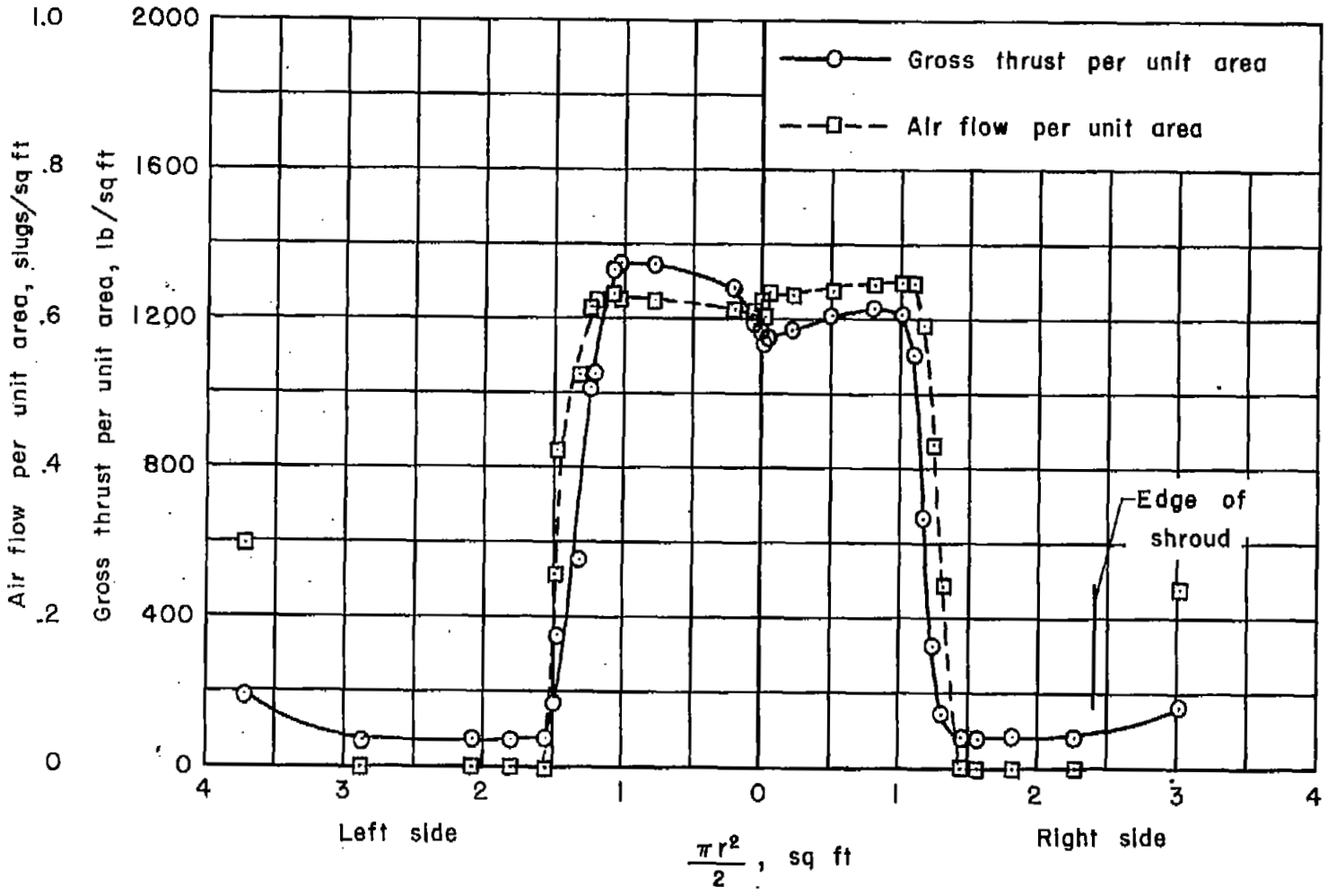

(a) Afterburner off; diameter ratio = 1.32; spacing ratio = 0.43.

Figure 8.- Typical thrust and air-flow profiles at the ejector exit; M = 0.75.

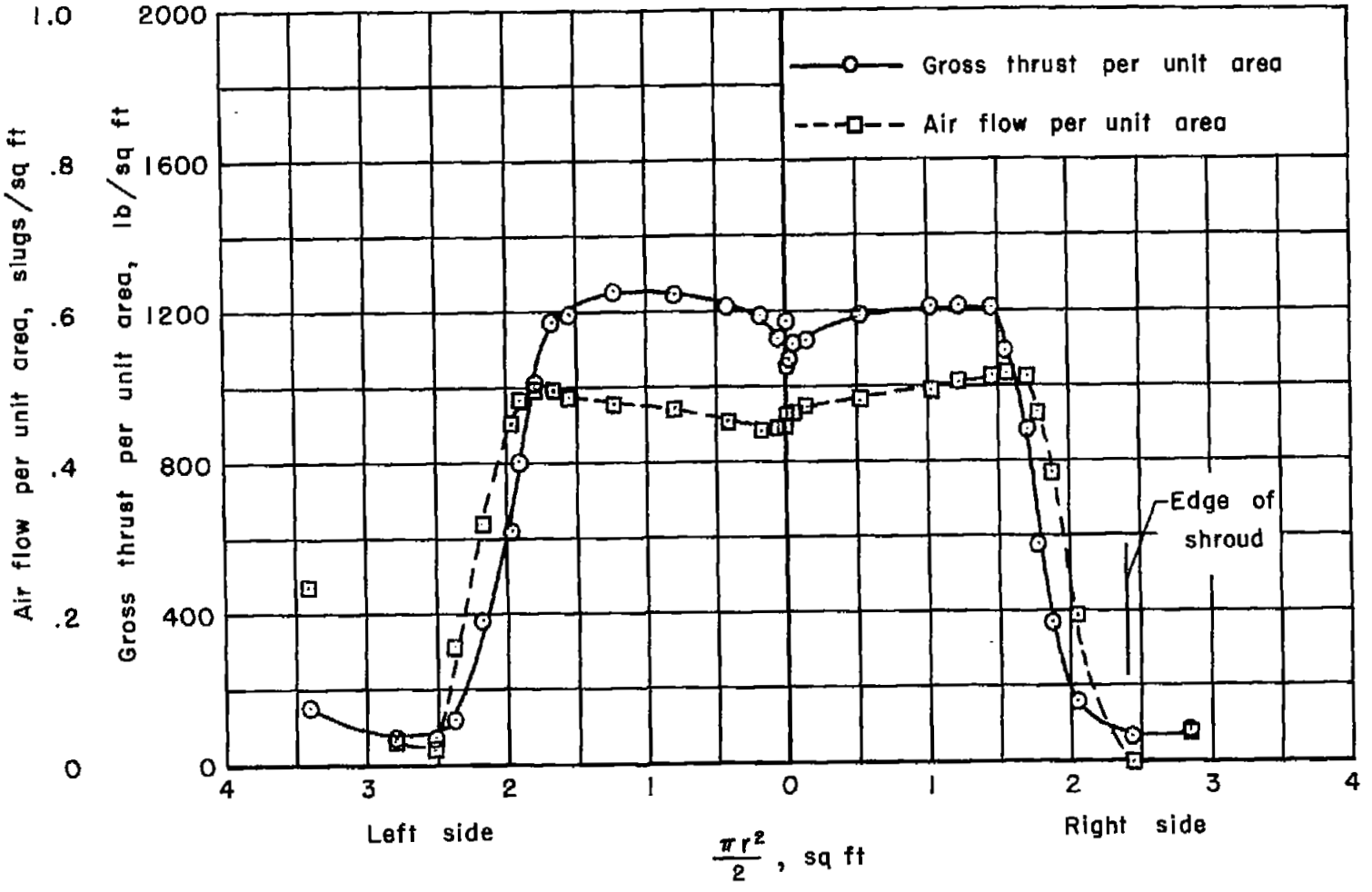

(b) Afterburner on; diameter ratio = 1.12; spacing ratio = 0.54.

Figure 8.- Concluded.

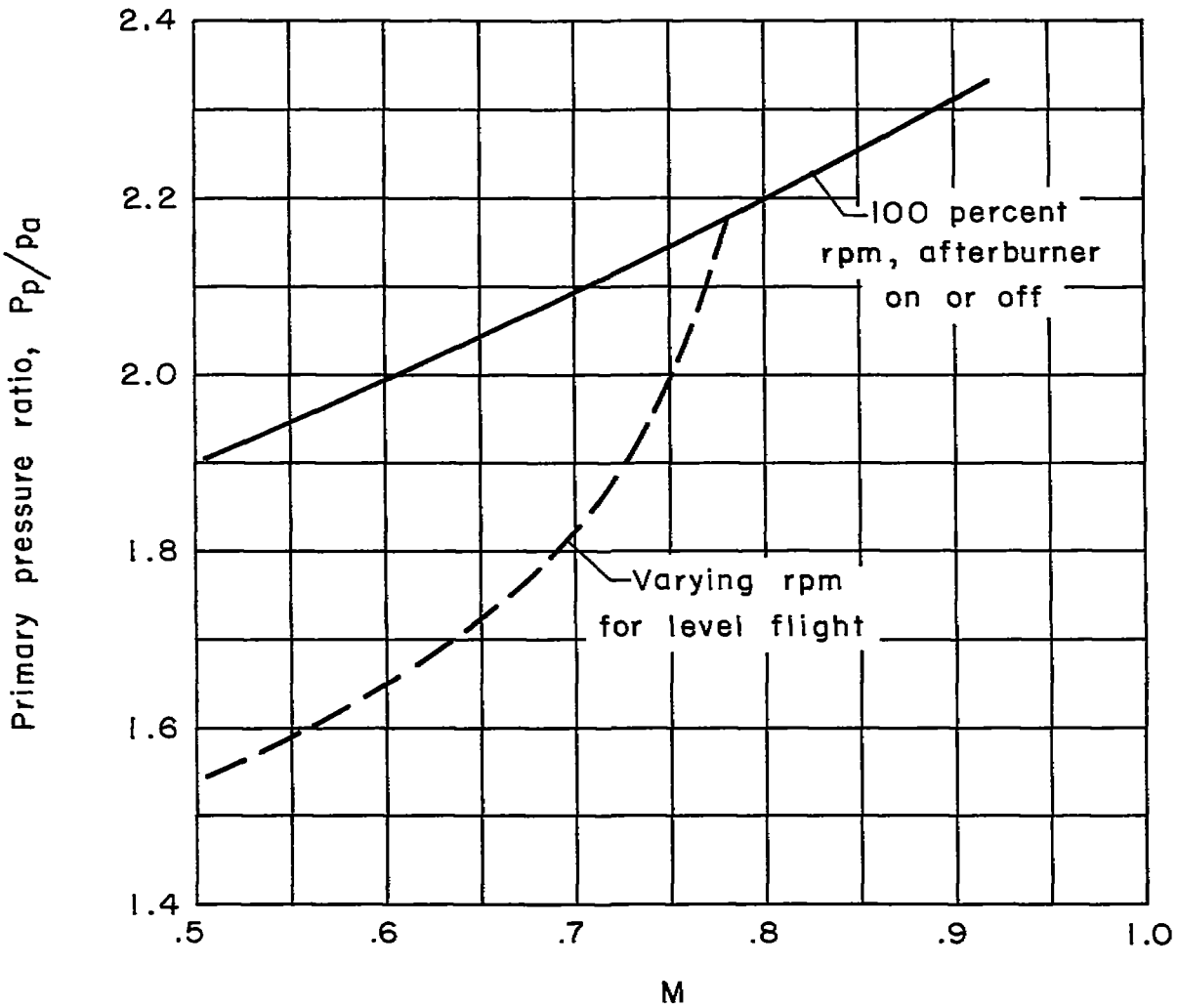

Figure 9.- Variation of the primary pressure ratio with flight Mach number.

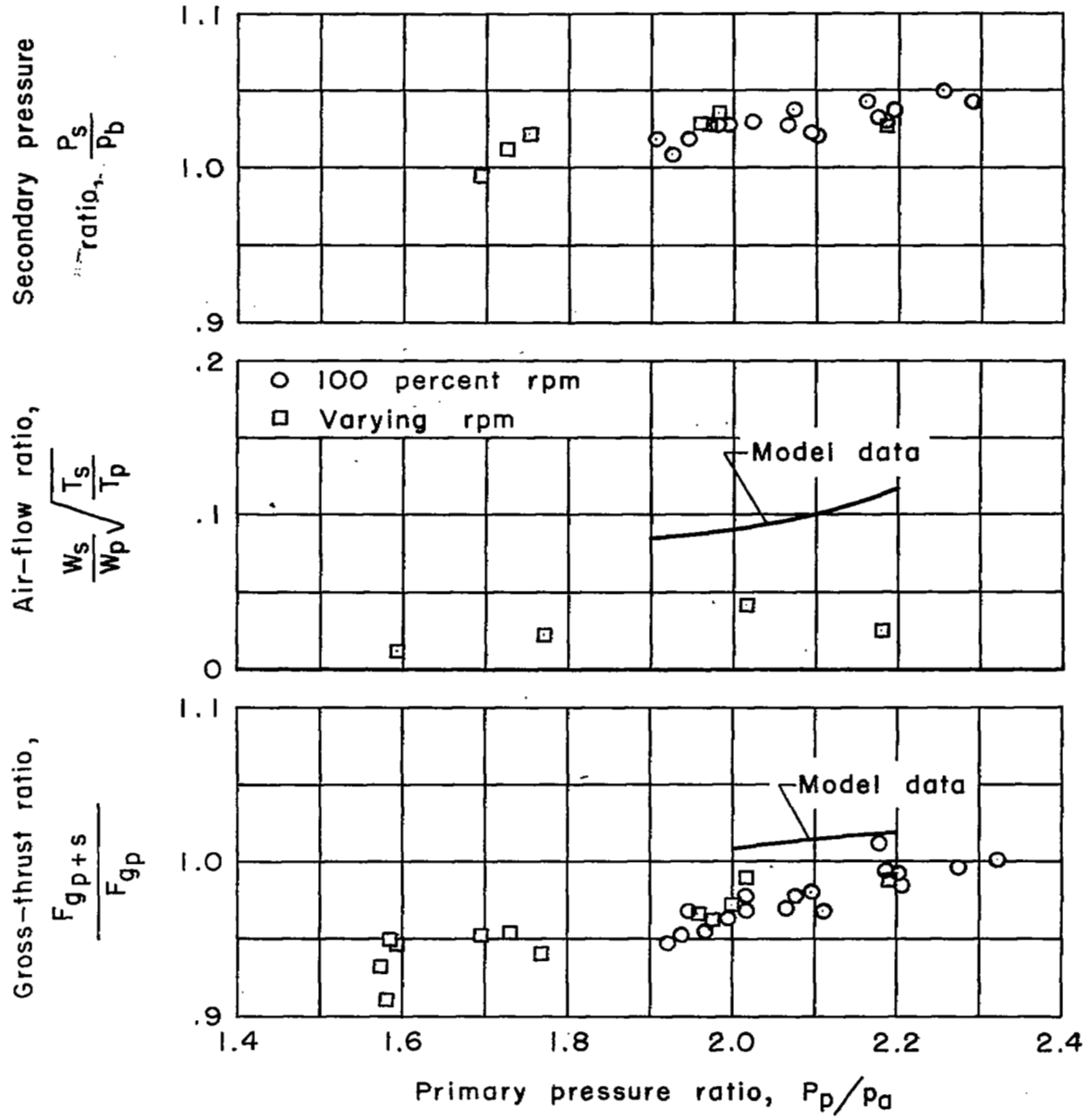

(a) Diameter ratio = 1.32; spacing ratio = 0.27.

Figure 10.- Ejector characteristics from flight tests and comparison with model tests; afterburner off, gap sealed.

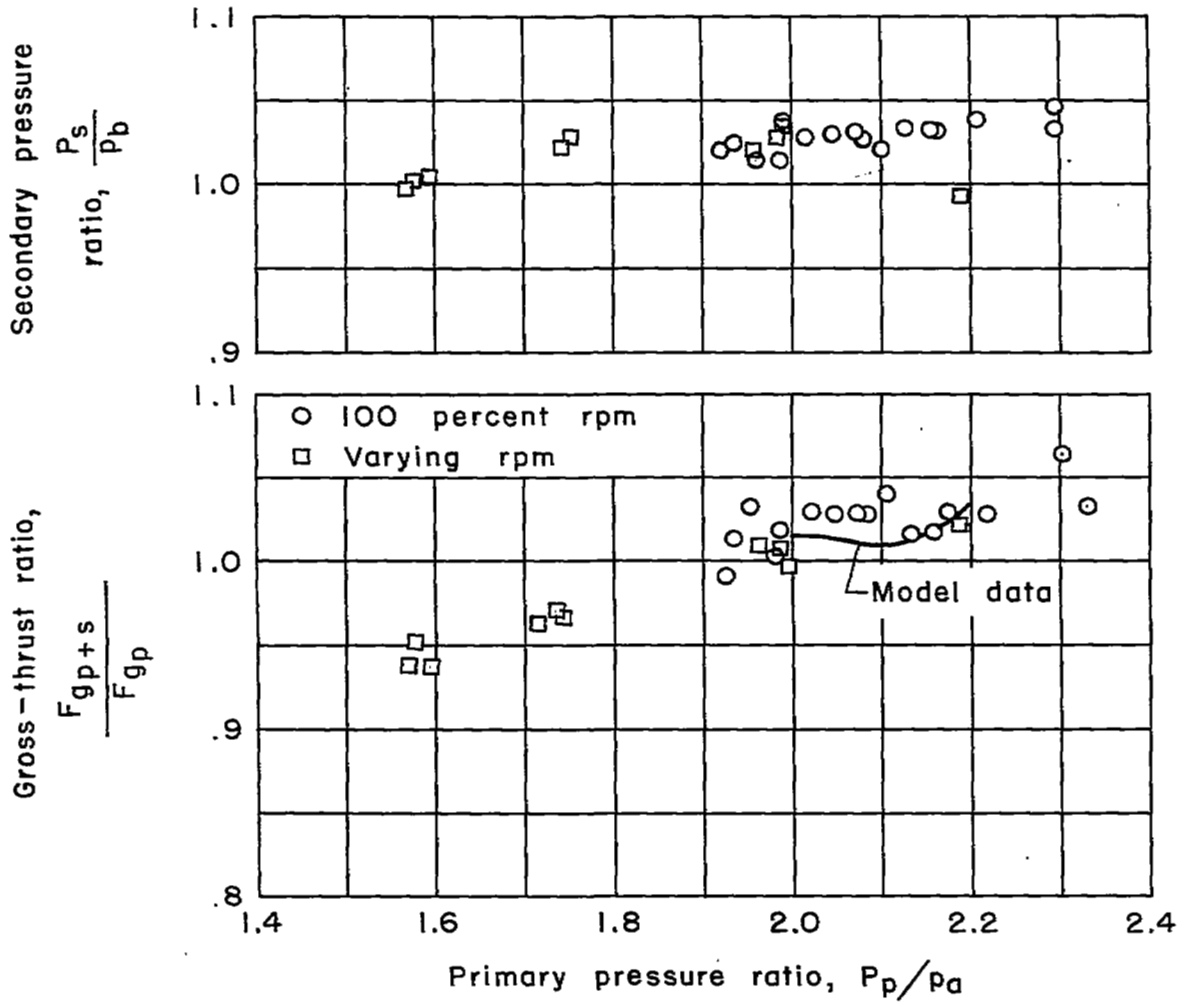

(b) Diameter ratio = 1.32; spacing ratio = 0.38.

Figure 10.- Continued.

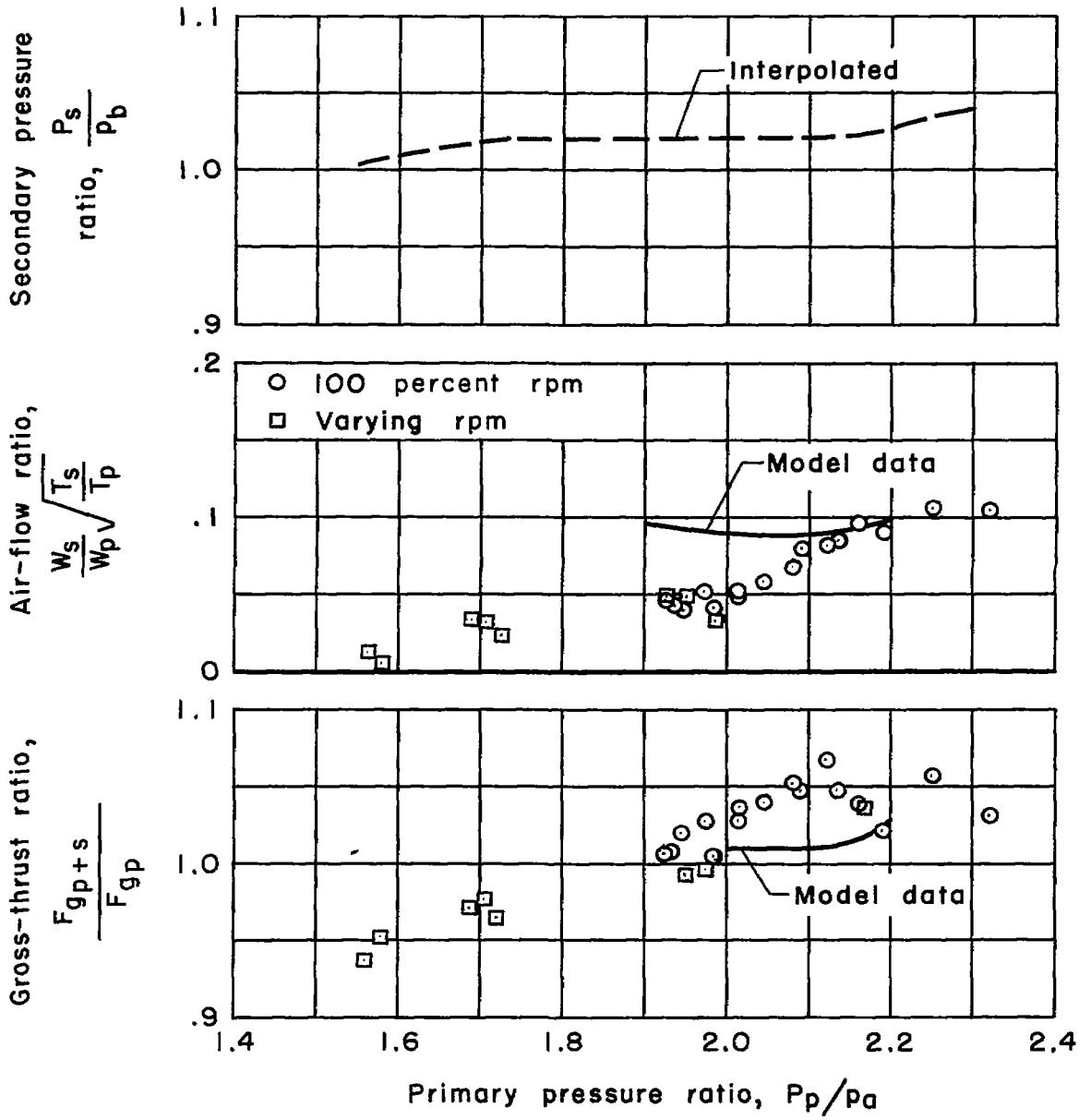

(c) Diameter ratio = 1.32; spacing ratio = 0.43.

Figure 10.- Continued.

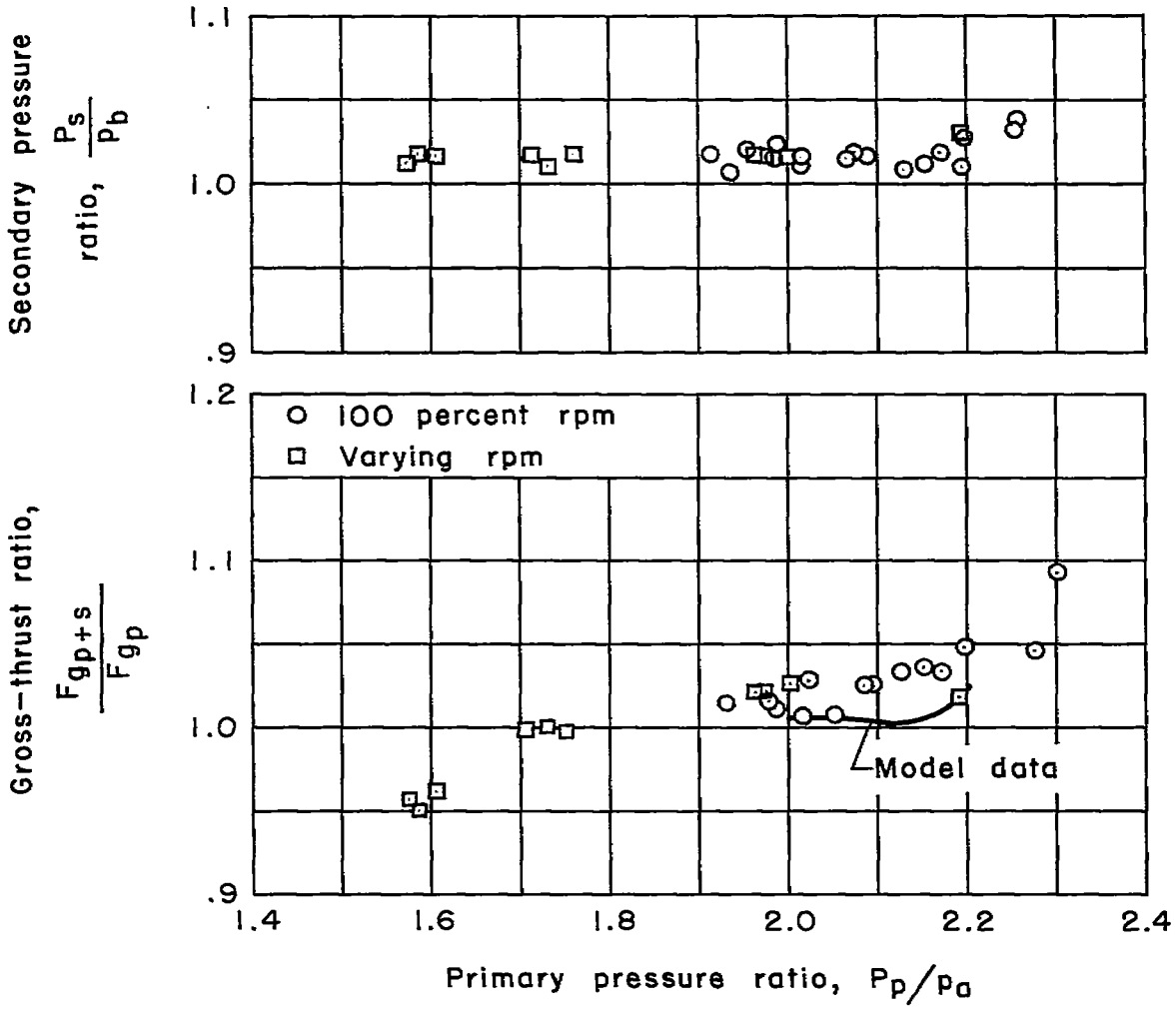

(d) Diameter ratio = 1.32; spacing ratio = 0.50.

Figure 10.- Continued.

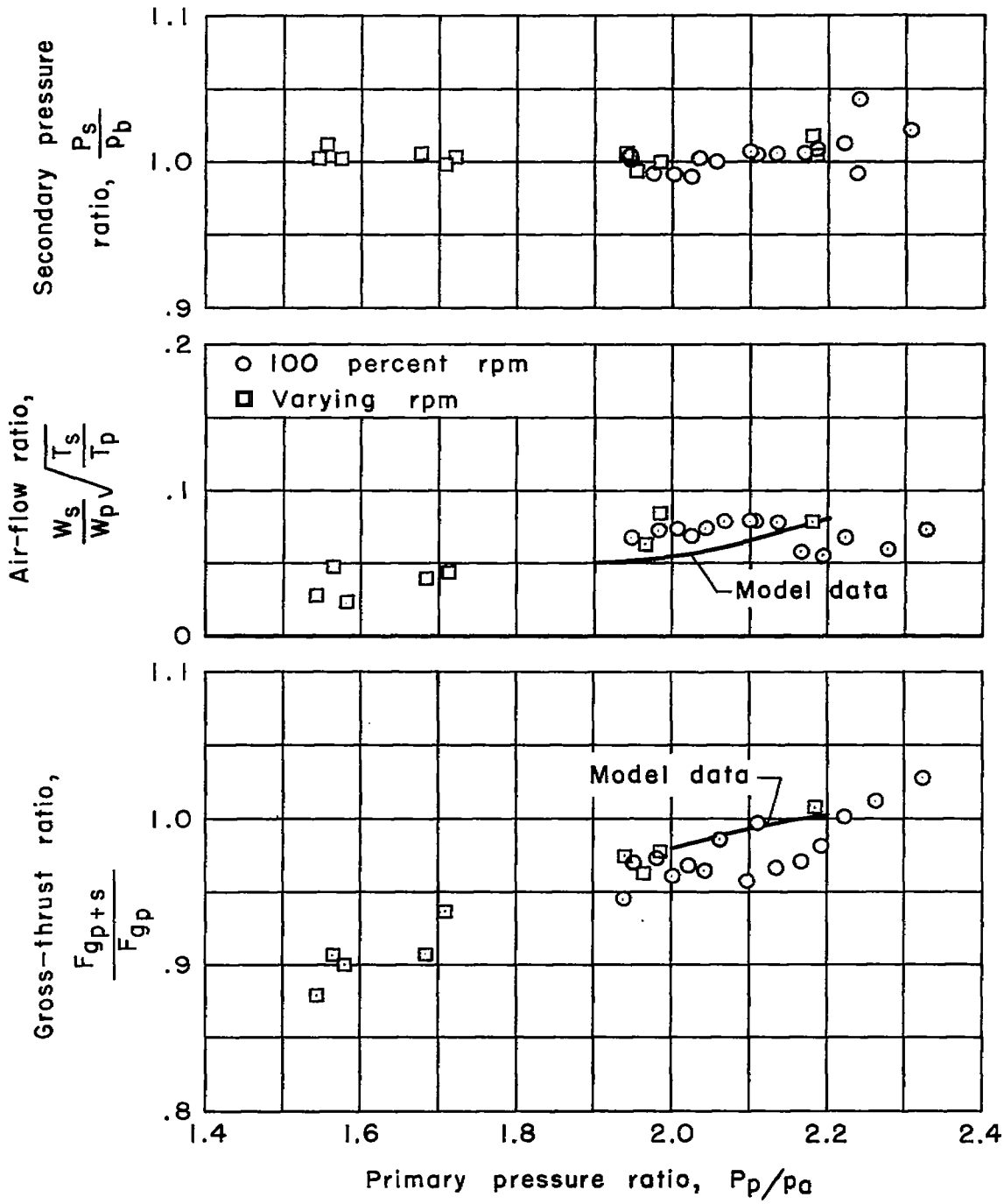

(e) Diameter ratio = 1.32; spacing ratio = 0.65.

Figure 10.- Concluded.

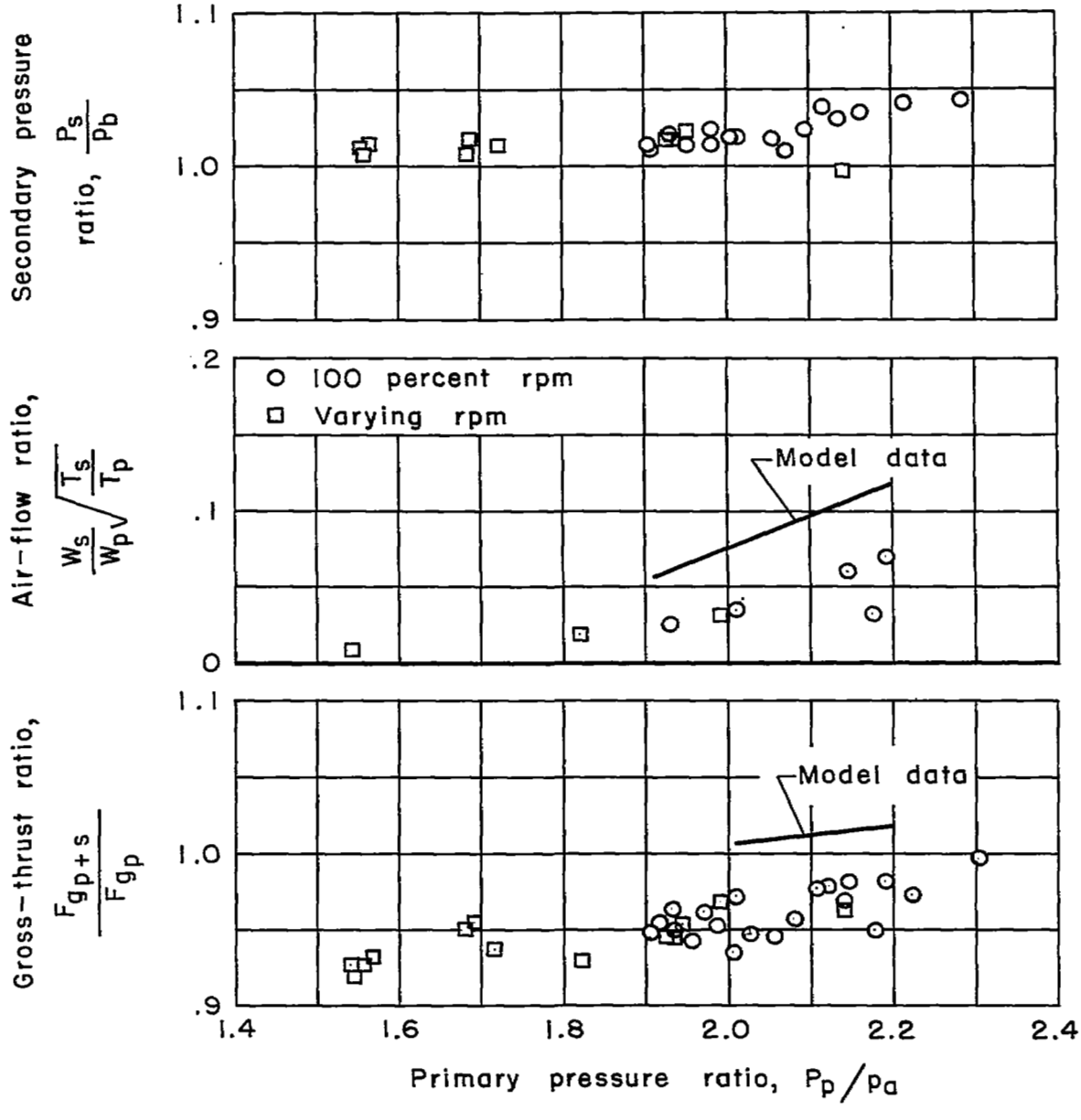

(a) Diameter ratio = 1.32; spacing ratio = 0.27.

Figure 11.- Ejector characteristics from flight tests and comparison with model tests; afterburner off, gap unsealed.

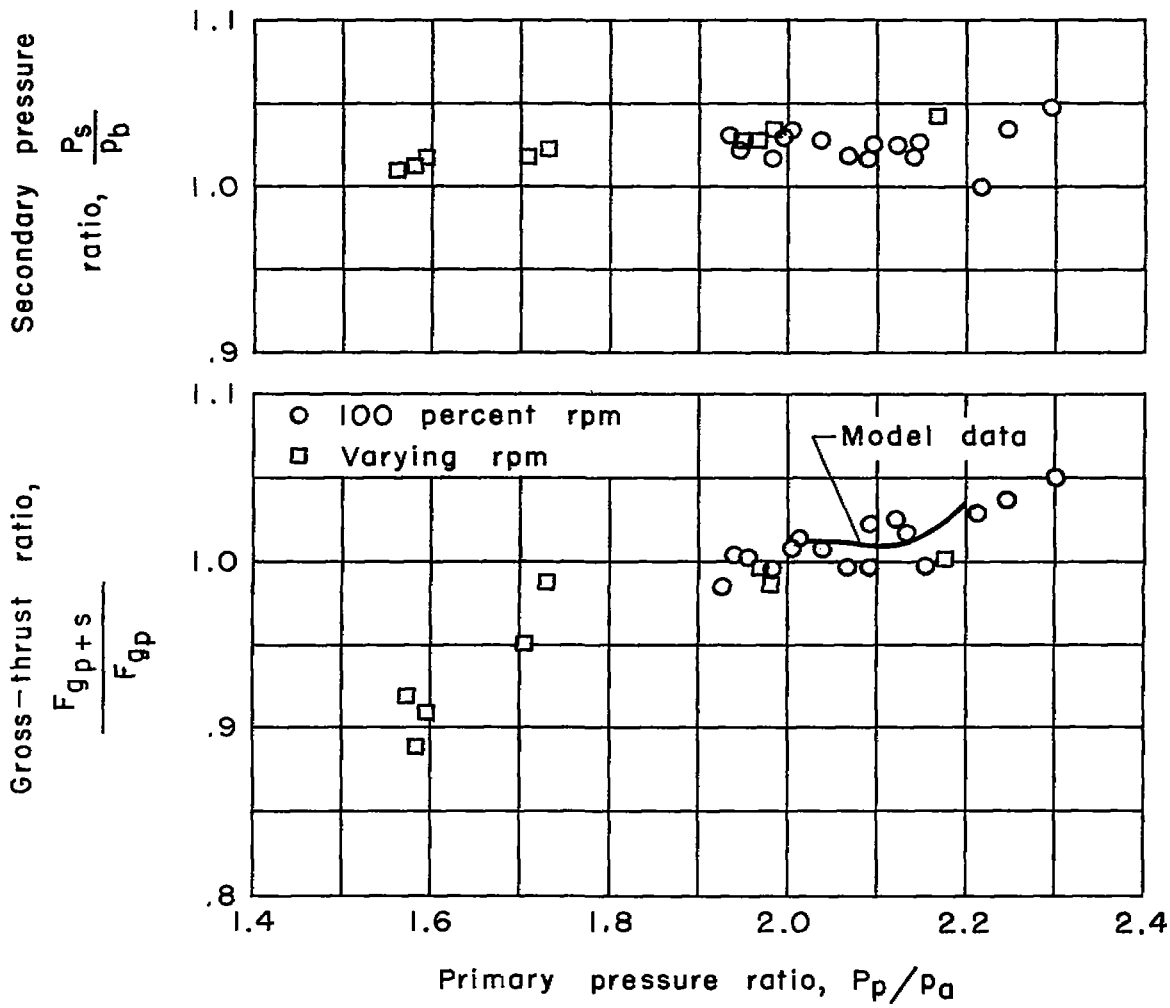

(b) Diameter ratio = 1.32; spacing ratio = 0.38.

Figure 11.- Continued.

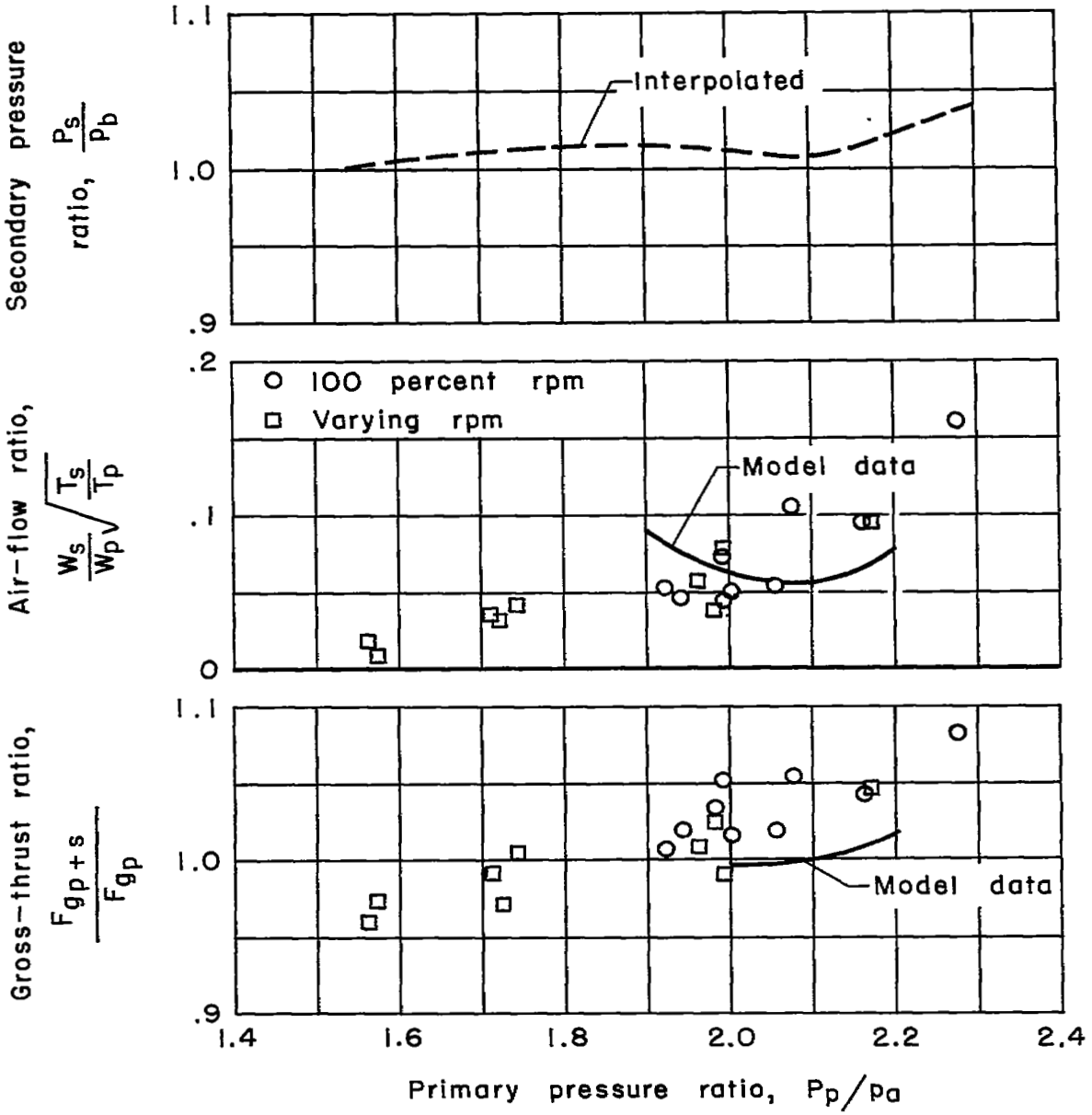

(c) Diameter ratio = 1.32; spacing ratio = 0.43.

Figure 11.- Continued.

[redacted]

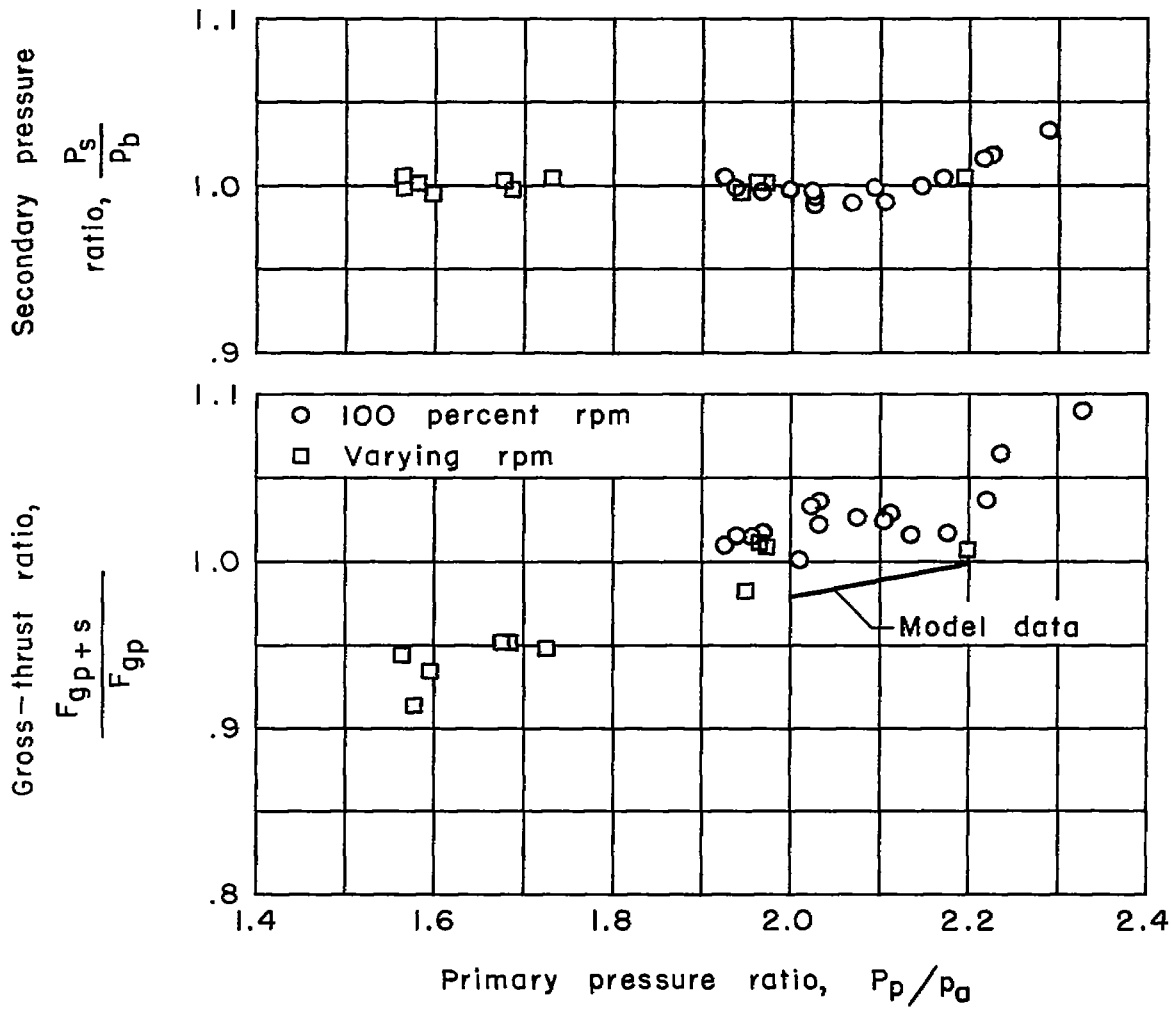

(d) Diameter ratio = 1.32; spacing ratio = 0.50.

Figure 11.- Continued.

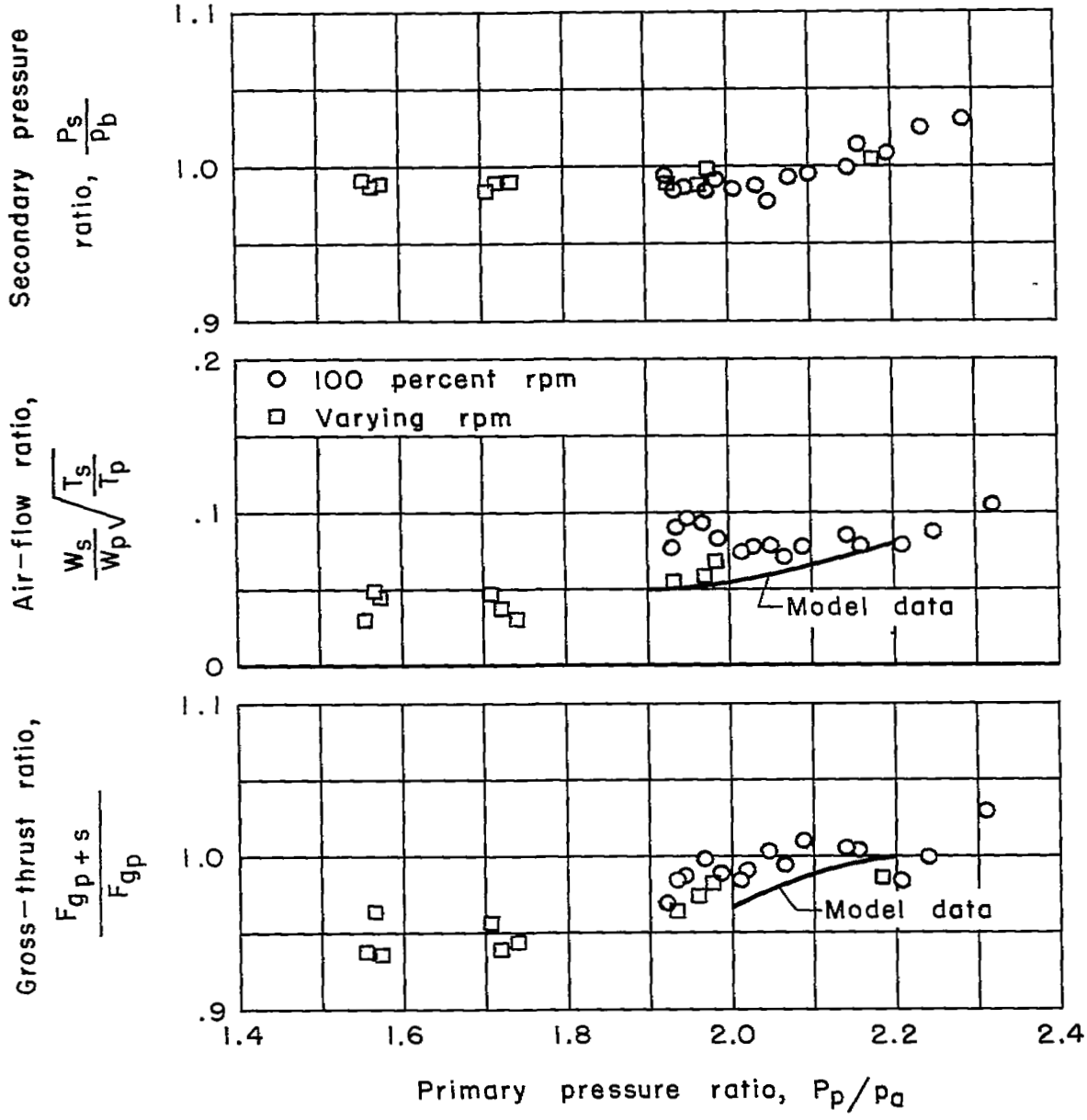

(e) Diameter ratio = 1.32; spacing ratio = 0.65.

Figure 11.- Concluded.

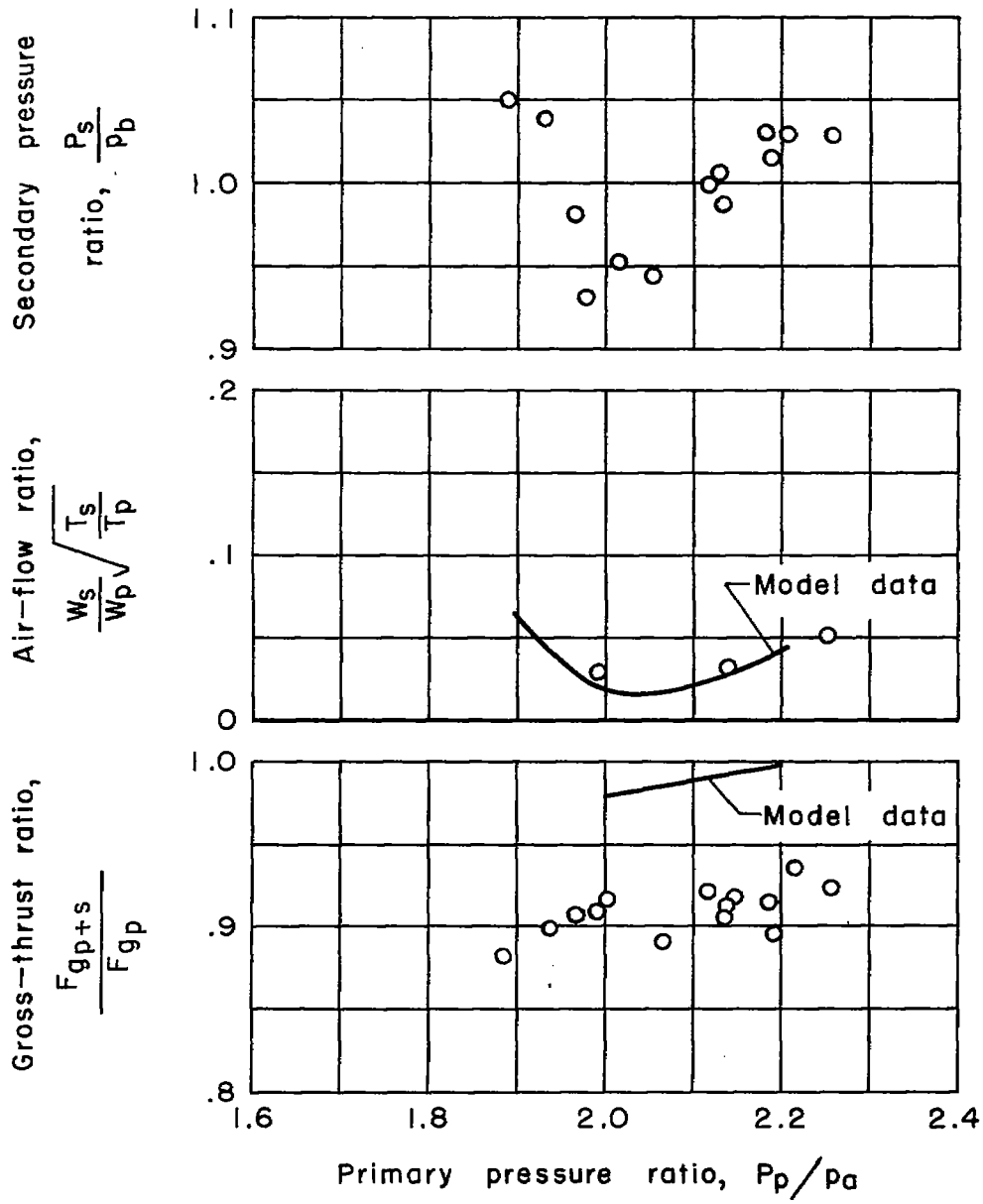

(a) Diameter ratio = 1.12; spacing ratio = 0.40.

Figure 12.- Ejector characteristics from flight tests and comparison with model tests; afterburner on, gap sealed.

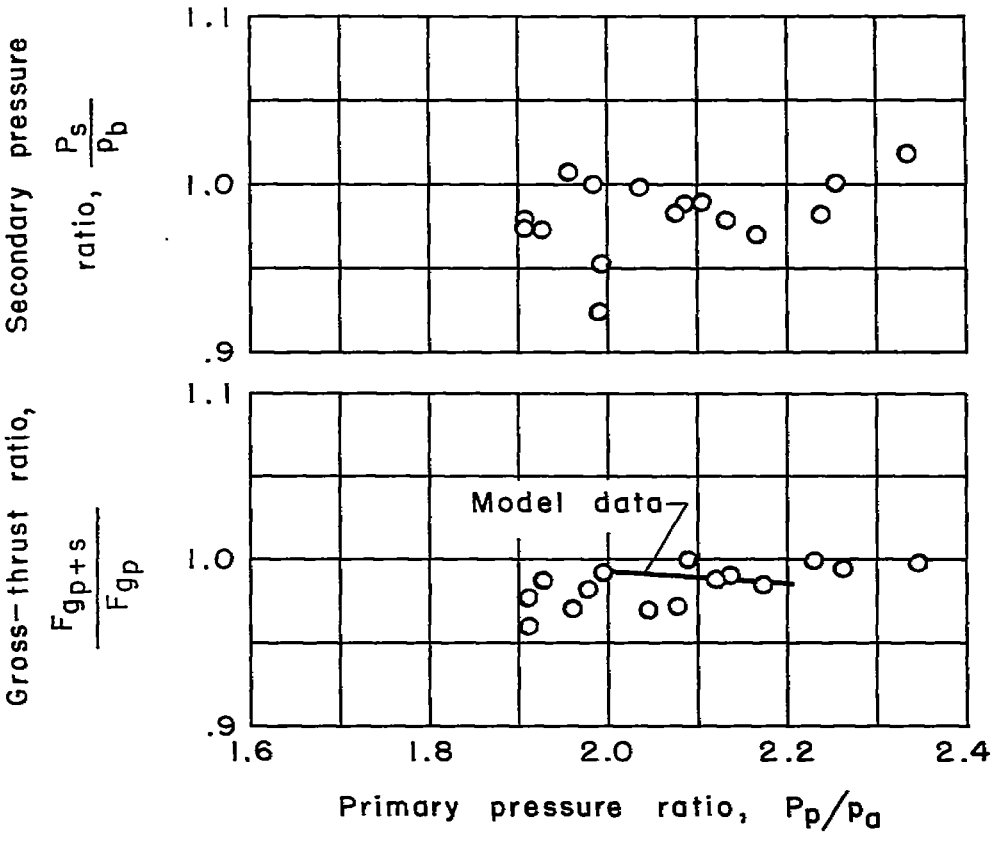

(b) Diameter ratio = 1.12; spacing ratio = 0.49.

Figure 12.- Continued.

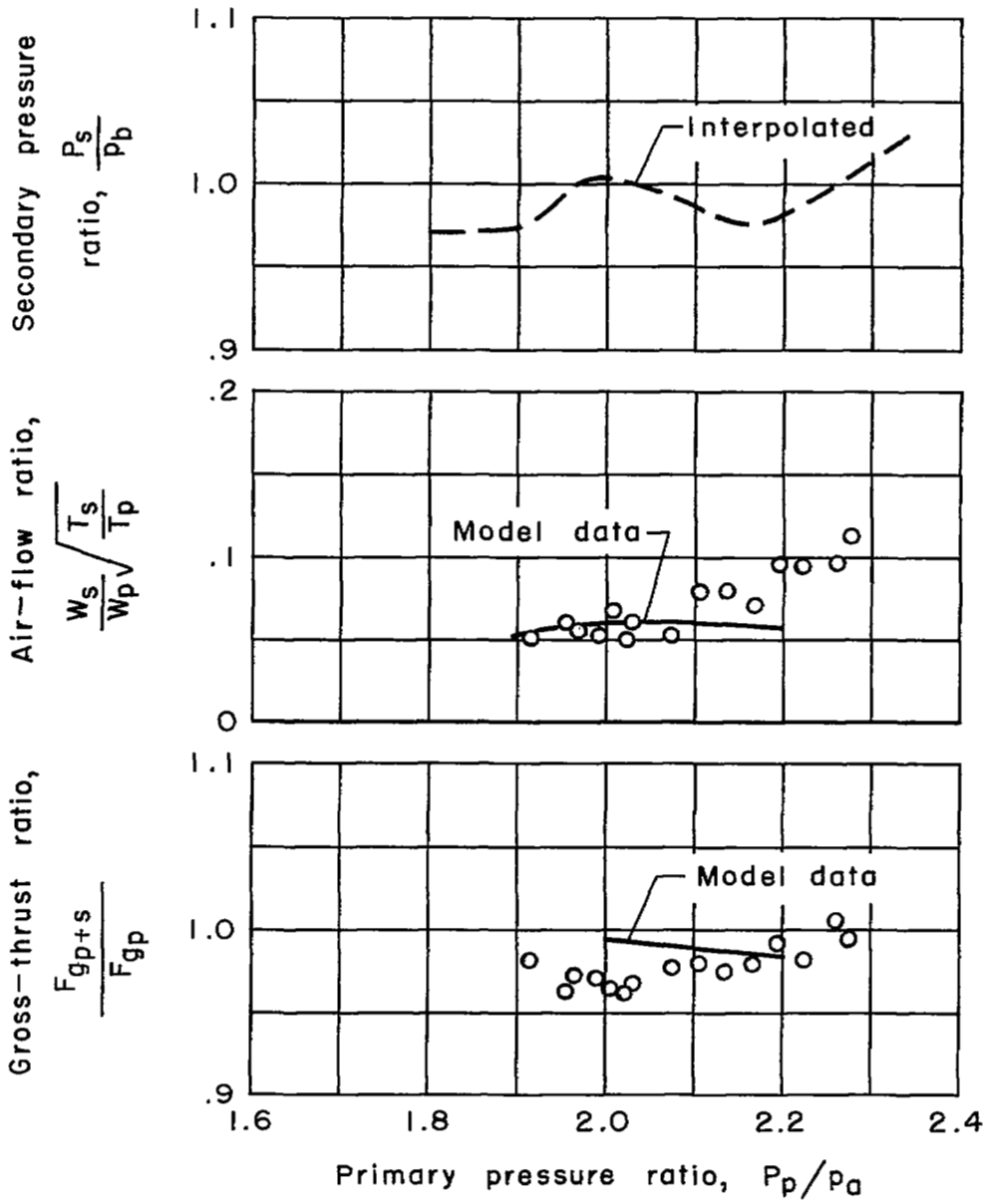

(c) Diameter ratio = 1.12; spacing ratio = 0.54.

Figure 12.- Continued.

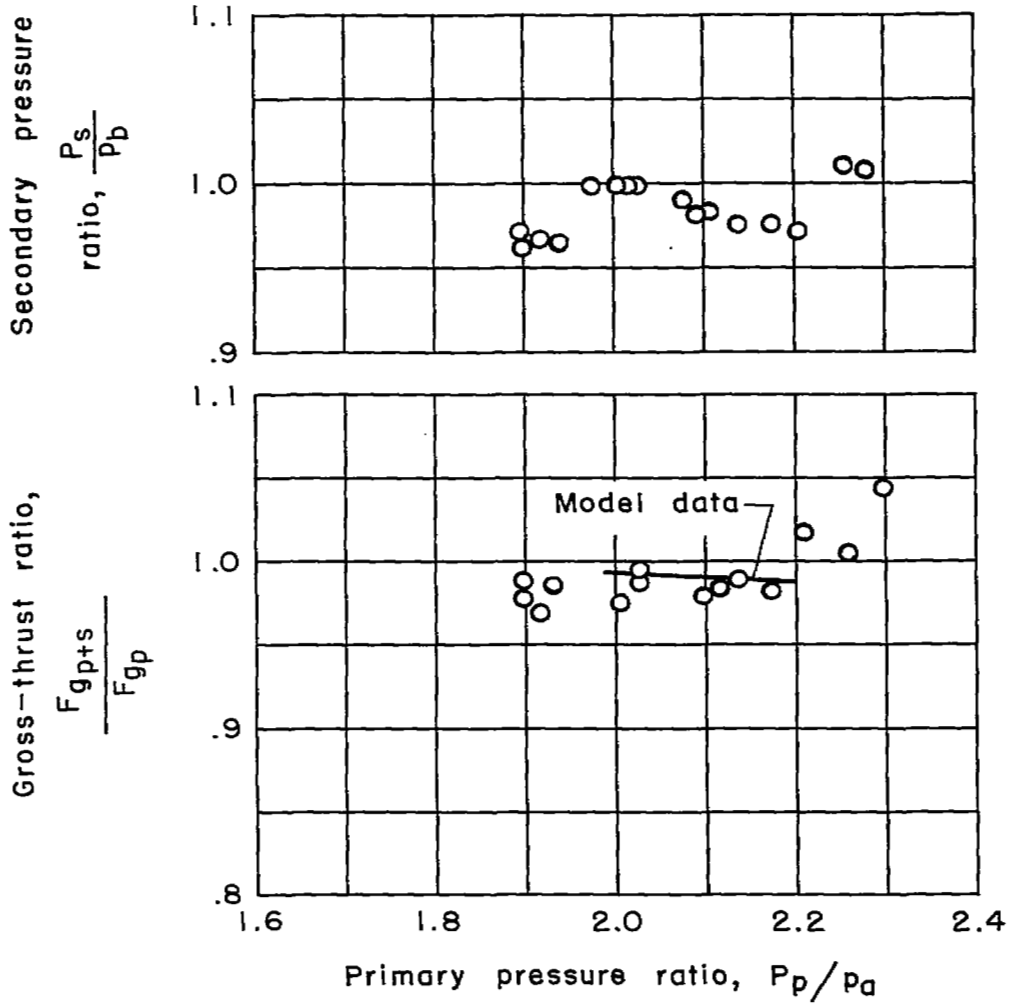

(d) Diameter ratio = 1.12; spacing ratio = 0.60.

Figure 12.- Continued.

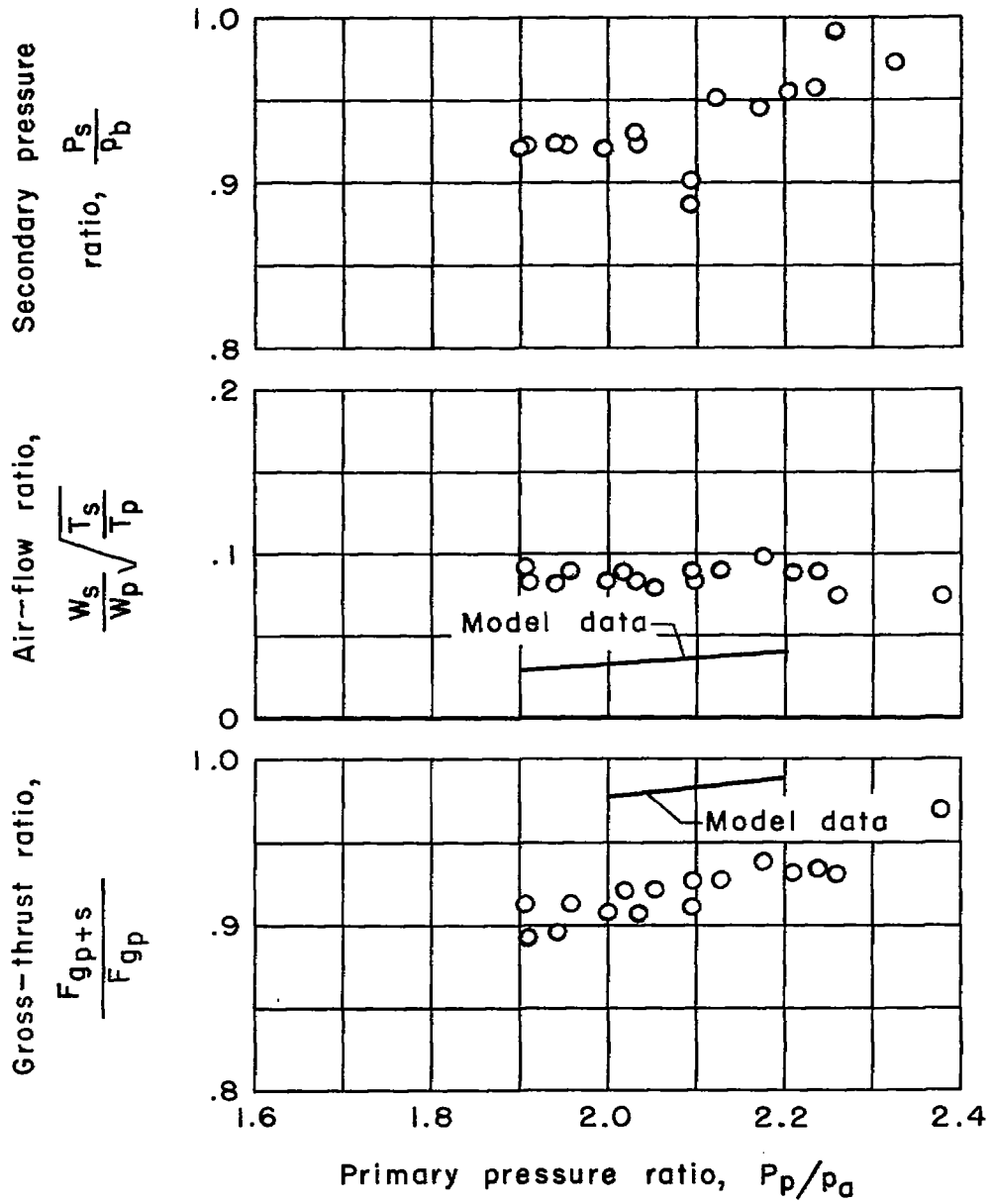

(e) Diameter ratio = 1.12; spacing ratio = 0.72.

Figure 12.- Concluded.

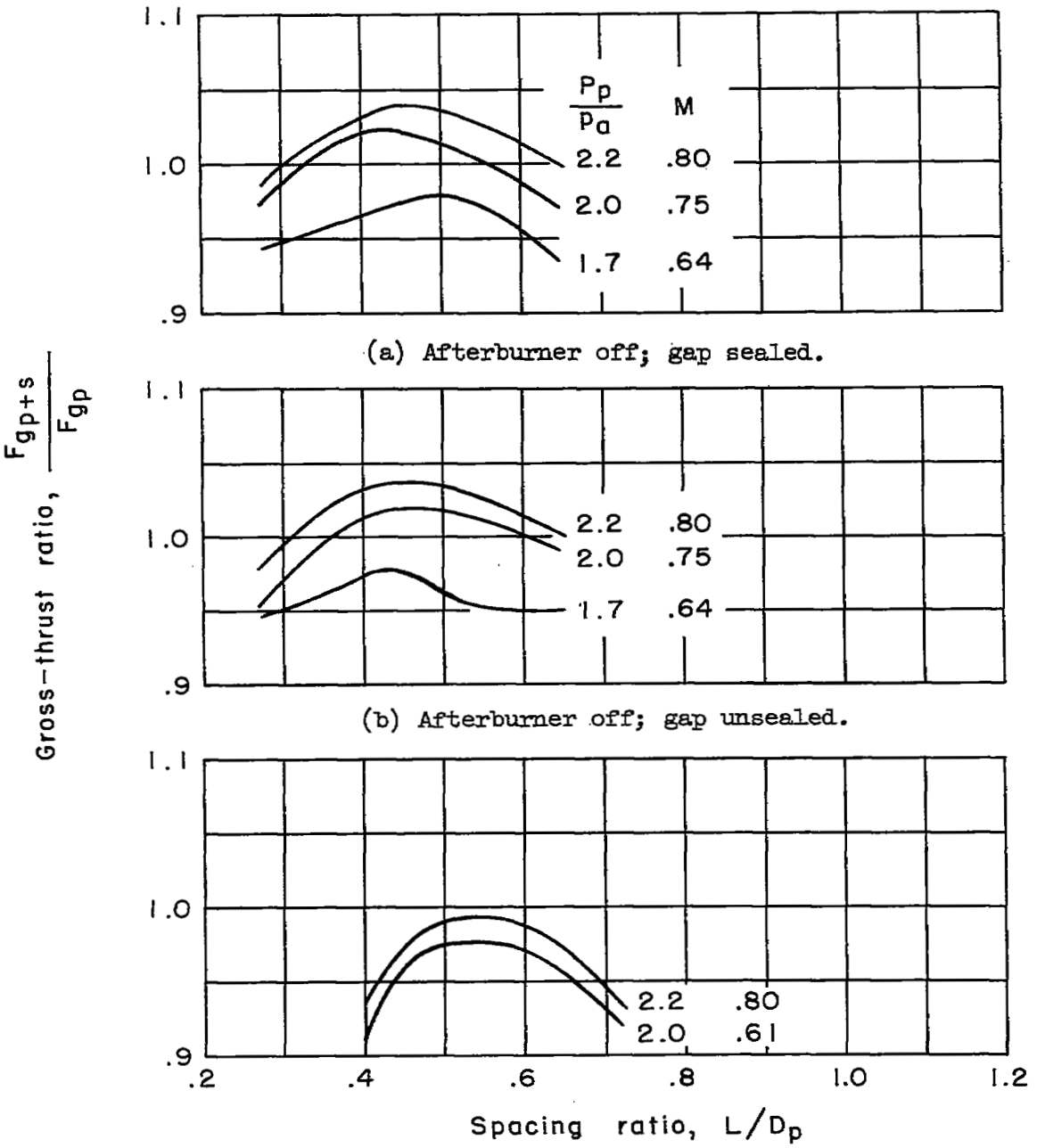

(a) Afterburner off; gap sealed.

(b) Afterburner off; gap unsealed.

(c) Afterburner on; gap sealed.

Figure 13.- Effect of spacing ratio on the gross-thrust ratio.

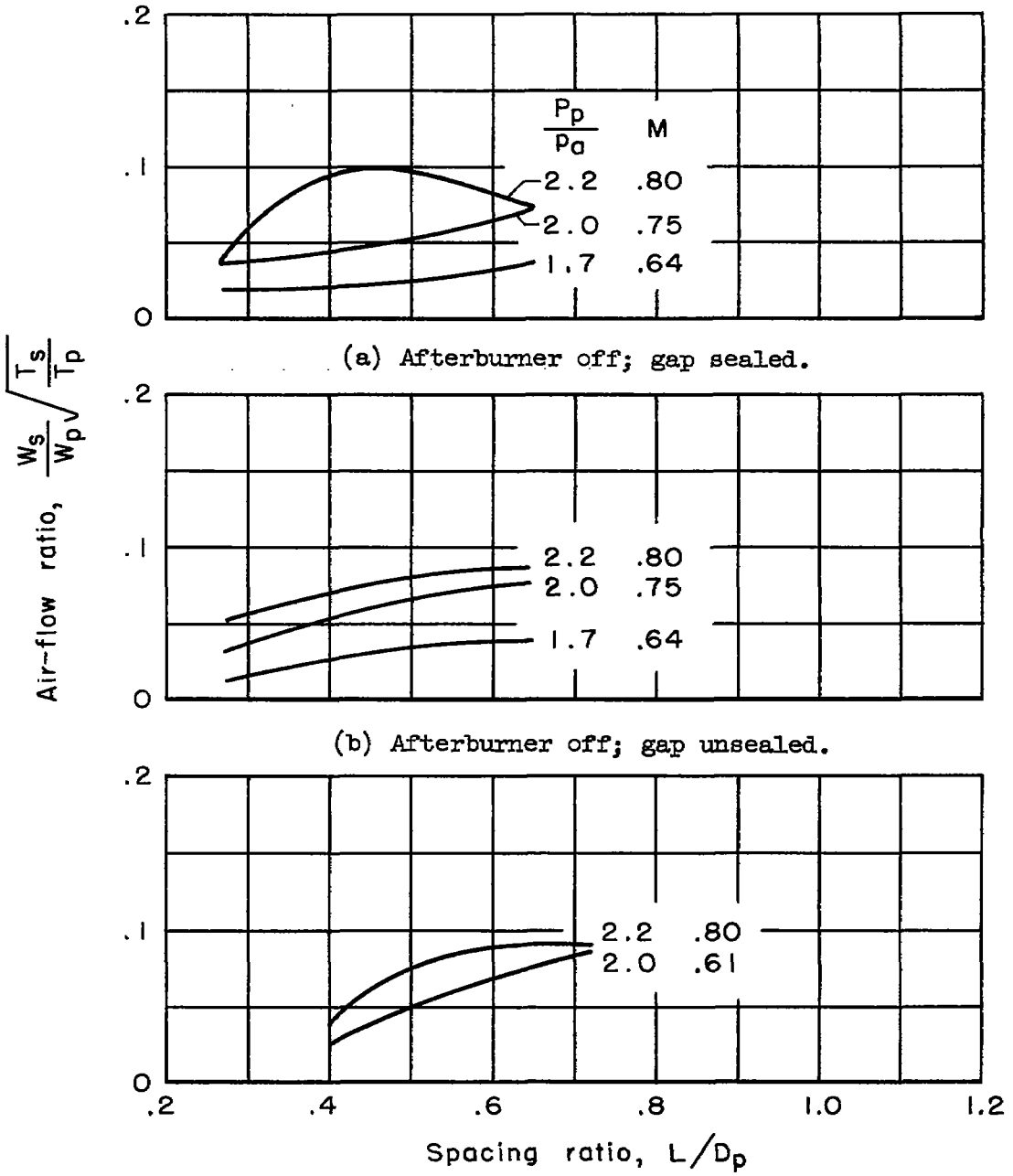

Figure 14.- Effect of spacing ratio on the ejector pumping characteristics.

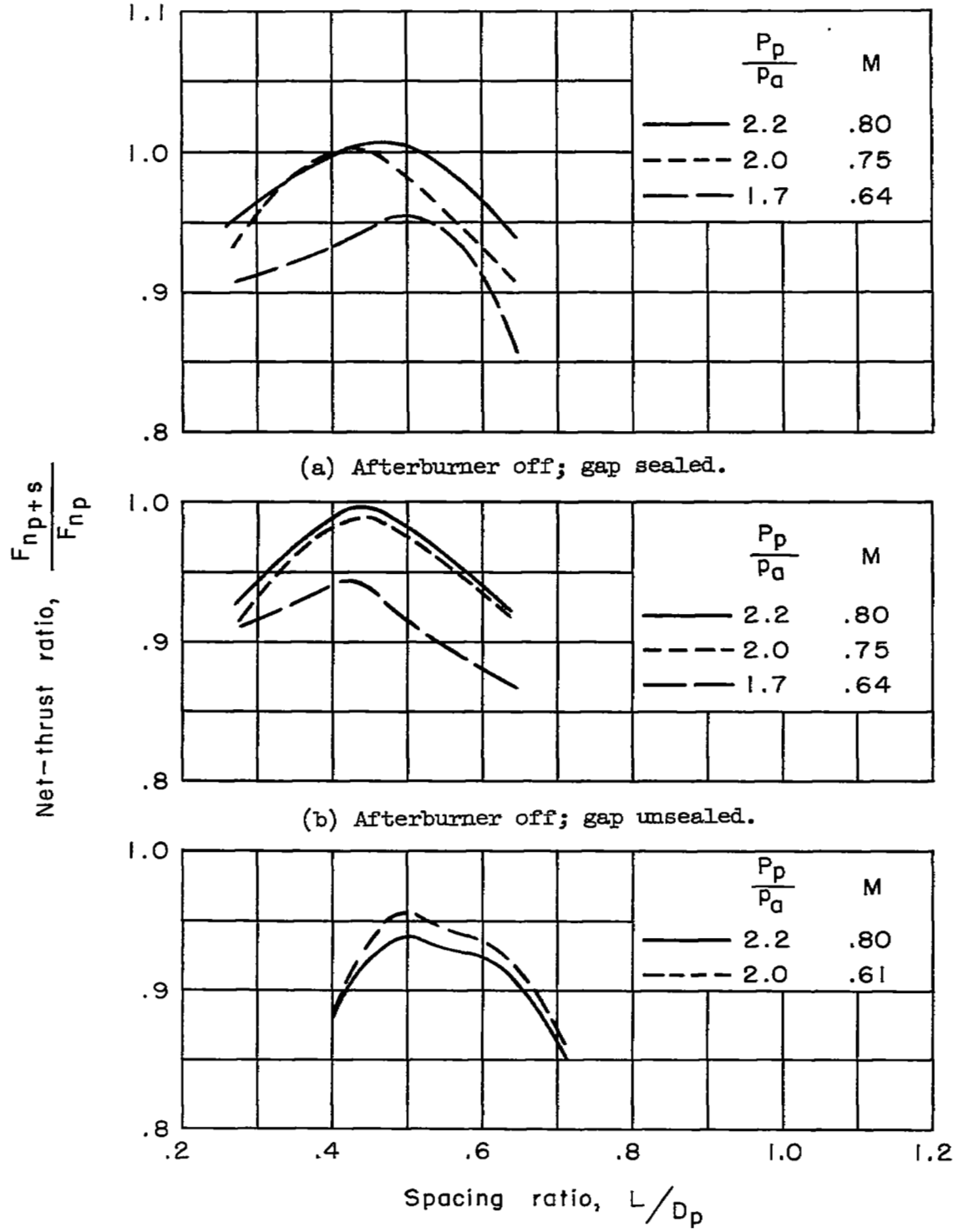

(a) Afterburner off; gap sealed.

(b) Afterburner off; gap unsealed.

(c) Afterburner on; gap sealed.

Figure 15.- Effect of spacing ratio on the net propulsive characteristics.

[redacted]

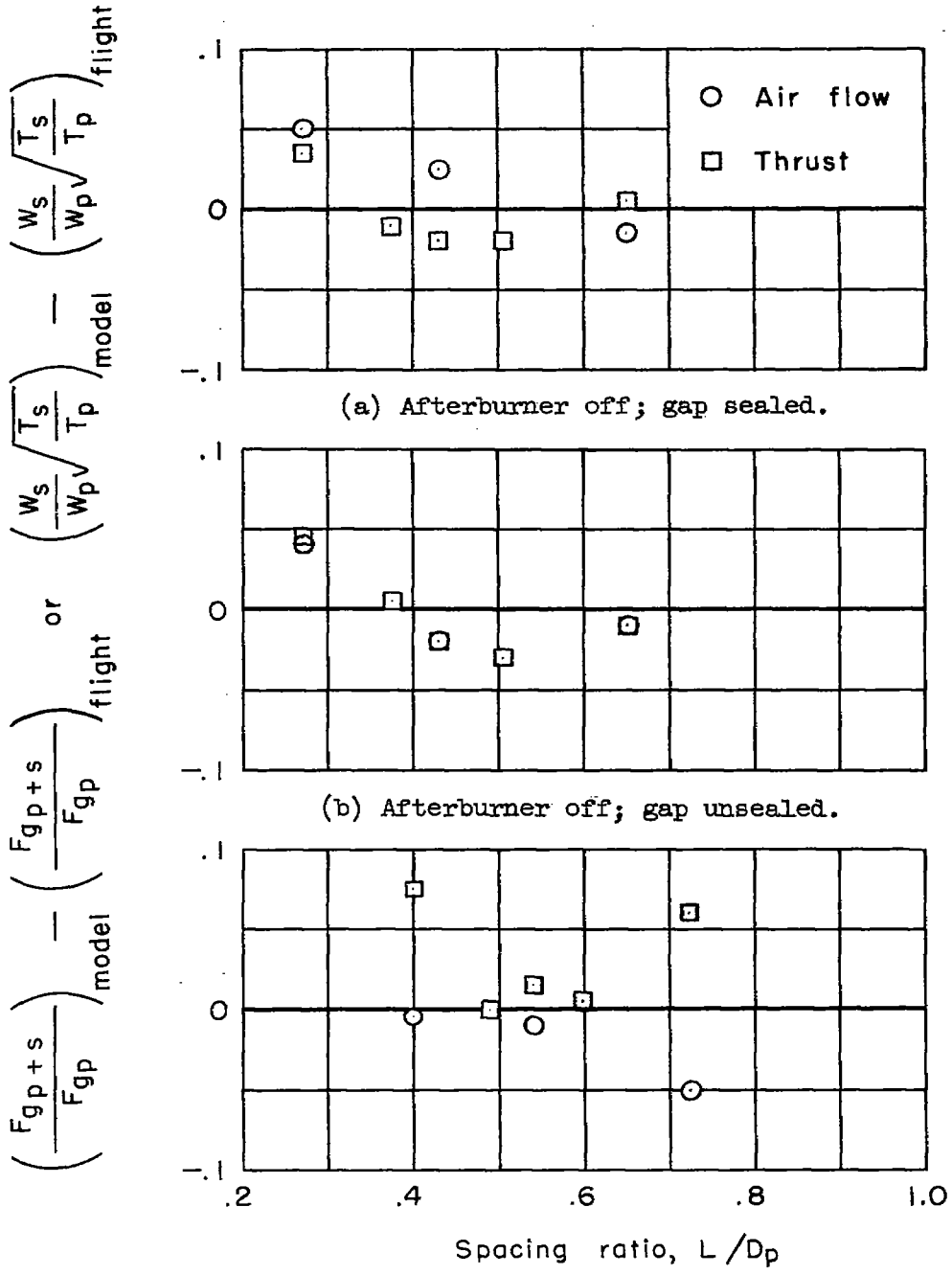

(a) Afterburner off; gap sealed.

(b) Afterburner off; gap unsealed.

(c) Afterburner on; gap sealed.

Figure 16.- Difference between flight and model data.

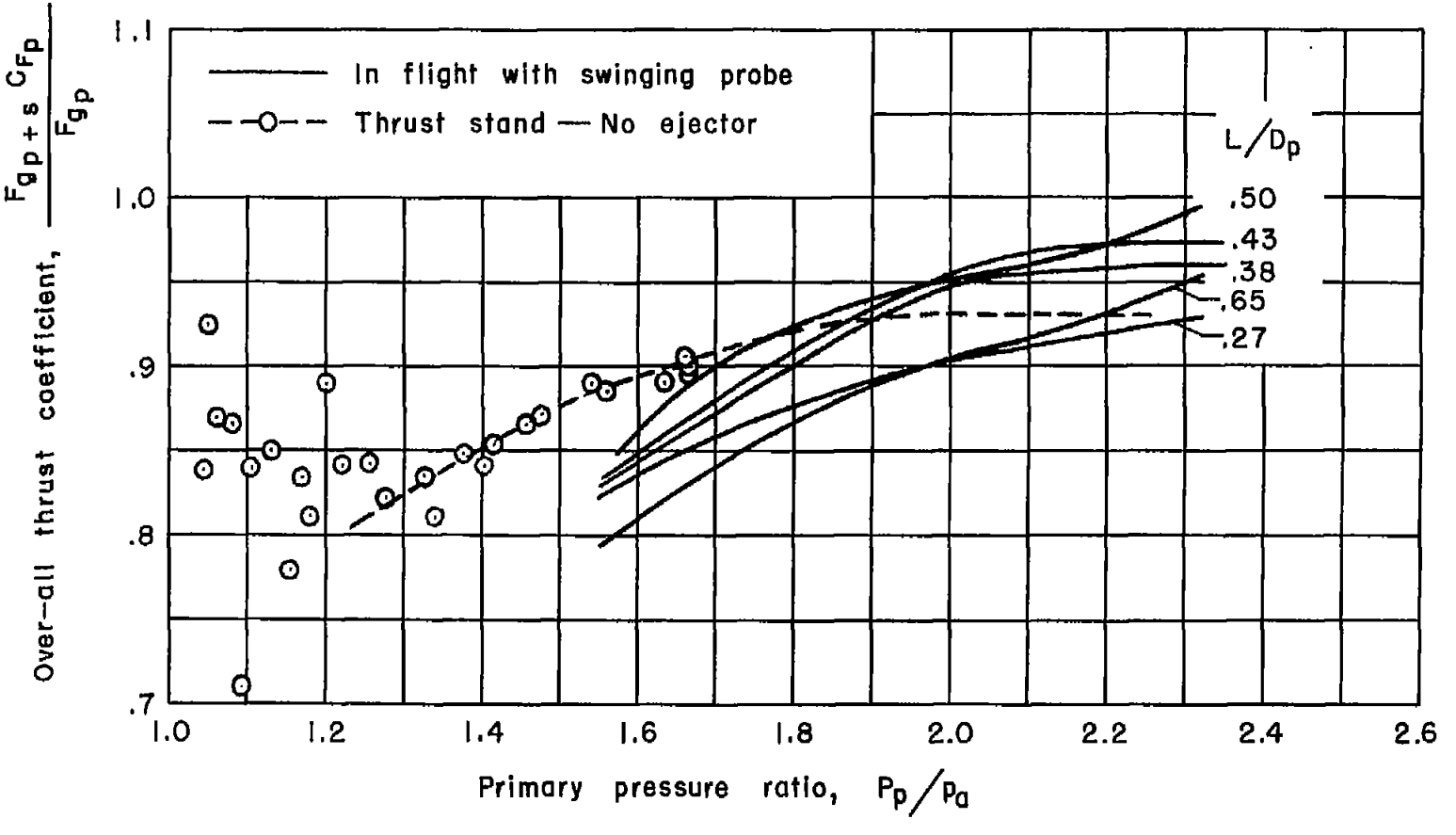

(a) Thrust coefficient.

Figure 17.- Over-all nozzle thrust and air-flow coefficients; afterburner off, gap sealed.

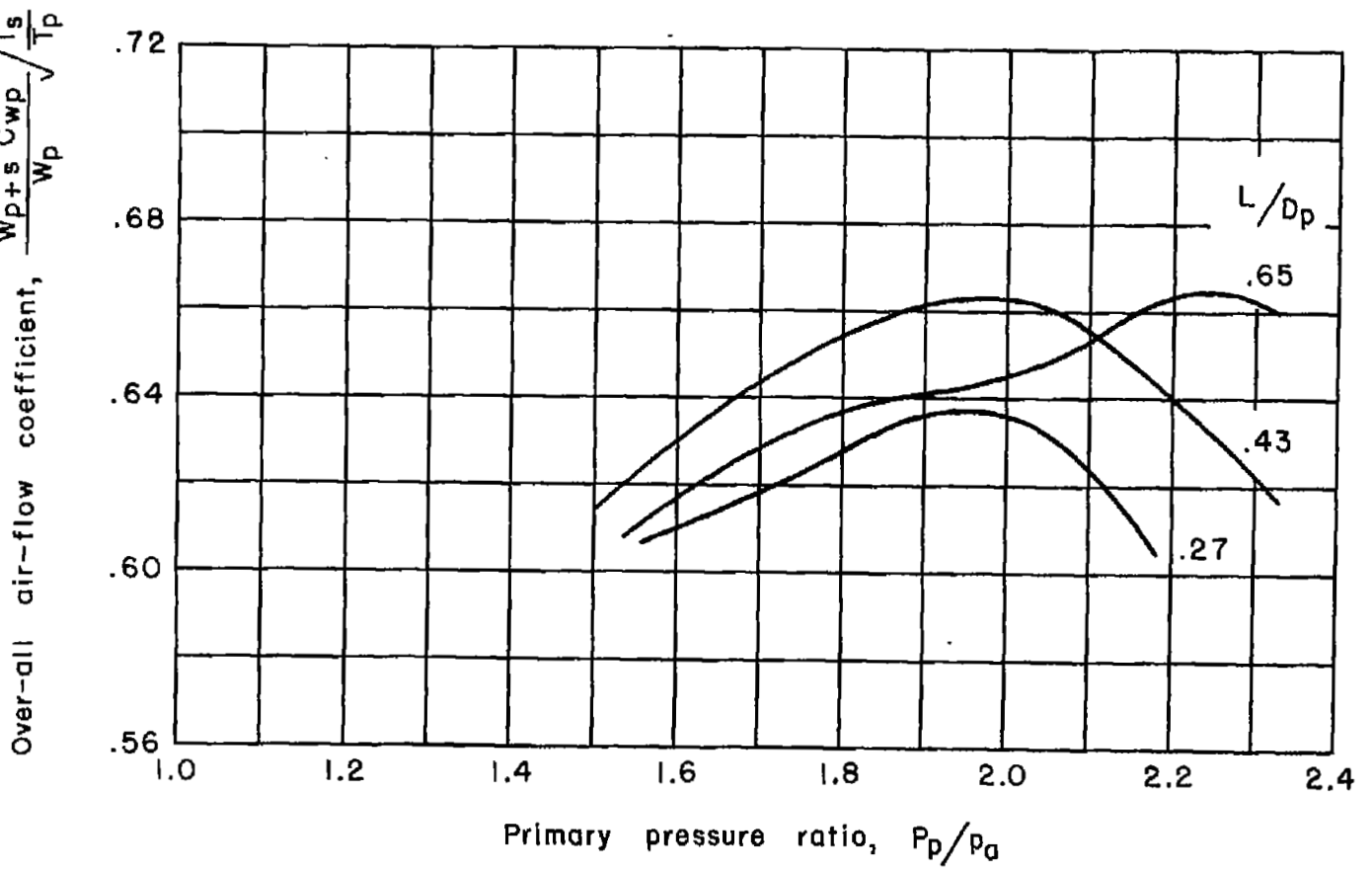

(b) Air-flow coefficient.

Figure 17.- Concluded.